

OPEN ACCESS

Review—Three Dimensional Zinc Oxide Nanostructures as an Active Site Platform for Biosensor: Recent Trend in Healthcare Diagnosis

To cite this article: Muhammad Luqman Mohd Napi *et al* 2020 *J. Electrochem. Soc.* **167** 137501


View the [article online](#) for updates and enhancements.



The banner features a background image of Earth from space. On the left, there are three circular logos: the ECS logo, the Electrochemical Society logo, and the Korean Electrochemical Society logo. The central text reads: "The best technical content in electrochemistry and solid state science and technology!" Below this, a blue bar contains the text "Available until November 9, 2020." On the right, the PRIME 2020 logo is displayed, with the text "PACIFIC RIM MEETING ON ELECTROCHEMICAL AND SOLID STATE SCIENCE" and "2020". At the bottom right, a dark blue box contains the text "REGISTER TO ACCESS CONTENT FOR FREE!" with a right-pointing arrow.



Review—Three Dimensional Zinc Oxide Nanostructures as an Active Site Platform for Biosensor: Recent Trend in Healthcare Diagnosis

Muhammad Luqman Mohd Napi,¹ Ahmad Fakhurrazi Ahmad Noorden,² Michael Loong Peng Tan,¹ Haryati Jamaluddin,³ Fatimah Abd Hamid,¹ Mohd Khairul Ahmad,⁴ Uda Hashim,⁵ Mohd Ridzuan Ahmad,⁶ and Suhana Mohamed Sultan^{1,2} 

¹Computational Nanoelectronic Research Lab, School of Electrical Engineering, Faculty of Engineering, Universiti Teknologi Malaysia, UTM Johor Bahru, 81310 Johor, Malaysia

²Advanced Optoelectronics Research Group (CAPTOR), Department of Physics, Kuliyah of Science, International Islamic University Malaysia, Bandar Indera Mahkota, 25200 Kuantan Pahang, Malaysia

³Department of Bioscience, Faculty of Science, Universiti Teknologi Malaysia, UTM Johor Bahru, 81310 Johor, Malaysia

⁴Microelectronics and Nanotechnology-Shamsuddin Research Centre (MiNT-SRC), Universiti Tun Hussein Onn Malaysia, Parit Raja 86400, Johor, Malaysia

⁵Institute of Nano Electronic Engineering, Universiti Malaysia Perlis, 01000, Kangar, Perlis, Malaysia

⁶Division of Control and Mechatronics Engineering, School of Electrical Engineering, Faculty of Engineering, Universiti Teknologi Malaysia, UTM Johor Bahru, 81310 Johor, Malaysia

Morphology effect is one of the essential factors that influence the performance of electrochemical biosensors based on ZnO nanostructures. These nanostructures are characterized by anisotropic growth with different dimensionalities such as zero-dimensional, one-dimensional, and two-dimensional. More interestingly, when combining each dimension into another advanced dimensionality, i.e. the three-dimensional (3-D), exceptional properties can be generated that are not otherwise found in low dimensionalities. The outstanding popularity of 3-D ZnO stems from many factors, with one of the most important being its synergic advantages from its low dimensional sub-unit and the additional surface area of the 3-D structure due to an increased geometric volume. This review briefly describes the principles and growth mechanism factors of 3-D ZnO via solution-based approaches and additional advanced methods. The paper further expands on the latest advancement of research into the 3-D ZnO nanostructure-based electrochemical biosensors to detect biomolecules that harm humankind. We also discussed the analytical performance of these biosensors using different nanocomposite materials. Additionally, limitations and suggestions on particular sensing works are proposed. Lastly, the five-year progress in research into 3-D ZnO-based electrochemical biosensors' performance in healthcare diagnosis is compared and future challenges presented.

© 2020 The Author(s). Published on behalf of The Electrochemical Society by IOP Publishing Limited. This is an open access article distributed under the terms of the Creative Commons Attribution 4.0 License (CC BY, <http://creativecommons.org/licenses/by/4.0/>), which permits unrestricted reuse of the work in any medium, provided the original work is properly cited. [DOI: 10.1149/1945-7111/abb4f4]



Manuscript submitted July 12, 2020; revised manuscript received August 19, 2020. Published September 14, 2020.

In recent years, the rapid development in zinc oxide nanostructure (ZnO) research has generated great interest in the construction of versatile nanostructure-based biosensors for medical diagnosis. The ZnO is one of the most promising nanomaterials for fabricating electrochemical biosensors because of its numerous unique features that can achieve single biomolecule detection.^{1,2} Previous works have successfully proven this unique feature, demonstrating success in determining various biomolecules such as glucose,³ cholesterol,⁴ cardiac Troponin-T (cTnT),⁵ uric acid,⁶ the Zika virus⁷ and nucleic acid.⁸ Interestingly, ZnO nanostructures can be synthesised via various methods that result in different morphologies.^{9–12} Of the diverse architectures of ZnO topography, hierarchical structures offer the most unique properties due to their three-dimensionalities. With increased geometric volume, strong binding properties, and an increased sensing surface, 3-D ZnO offers greatly improved sensitivity and efficiency in detecting.^{13–15}

Basically, the electrochemical biosensors is formed via three main electrodes, which are the working electrode, the counter electrode, and the reference electrode (Figs. 1a–1c). The working electrode consists of a conductive electrode with a bioreceptor that serves as a probe immobilised on its surface. The working mechanism of electrochemical biosensors is based on the electroanalytical method. When the biomolecules' target approaches the working electrode, it will have an induced change lending it an electrochemical behaviour that is directly converted into an electrical signal.¹⁶ Quantitative sensing can be done by controlling the potential of the electrode and measuring its current response.¹⁷ Electrochemical methods offer unique advantages such as fast-response detection, good sensitivity, and low-cost fabrication.^{18,19} Recently, electrochemical-based biosensing devices

have been reported to offer real-time monitoring and more ease of control compared to other biosensing techniques.²⁰

Nanostructures-based electrochemical biosensors have been widely used in healthcare diagnosis because of several advantages such as high sensitivity at low concentrations and ease of production.^{21,22} The performance of such sensors is significantly influenced by the topography of the sensing materials. Realising the importance of sensing materials, there has been an aggressive development in sensor morphological structures—zero-dimensional to three-dimensional—since over a decade ago.²³ Although significant works have reported the excellent performance of low-dimensional structures (0-D, 1-D, and 2-D) in biosensing applications, there is still room for improvements in this field. For example, 0-D ZnO is known to be an excellent sensing platform due to its large surface area.²⁴ However, 0-D ZnO has poor electron mobility caused by the many grain boundaries in the material that restrict electron transfer. Therefore, 1-D ZnO was produced to replace it.²⁵ The nanowire-based electrochemical biosensor is among the 1-D structures that possess a fast and stable, direct electron flow.²⁶ However, it also has a limited surface area and limited space to provide site immobilisation.²⁵ Meanwhile, the 2-D ZnO nanostructures offer higher specific area but the challenge issue in this case about to create planar nanoshape with minimal scattering.²⁵ Thus, 3-D ZnO was introduced, the unique morphology of which has opened up a whole new era in medical diagnostics research. These structures provide extra surface area due to an increased geometric volume, which makes them a better platform for immobilising bioreceptors. In addition, the 3-D ZnO is made up of low-dimensional nanostructures that offer greater novelty effects and properties and increased sensing performance. The development of 3-D ZnO materials for electrochemical-based biosensor fabrication including their advance structure device (Fig. 1d) is now becoming the focus of much research.

²E-mail: suhasultan@utm.my

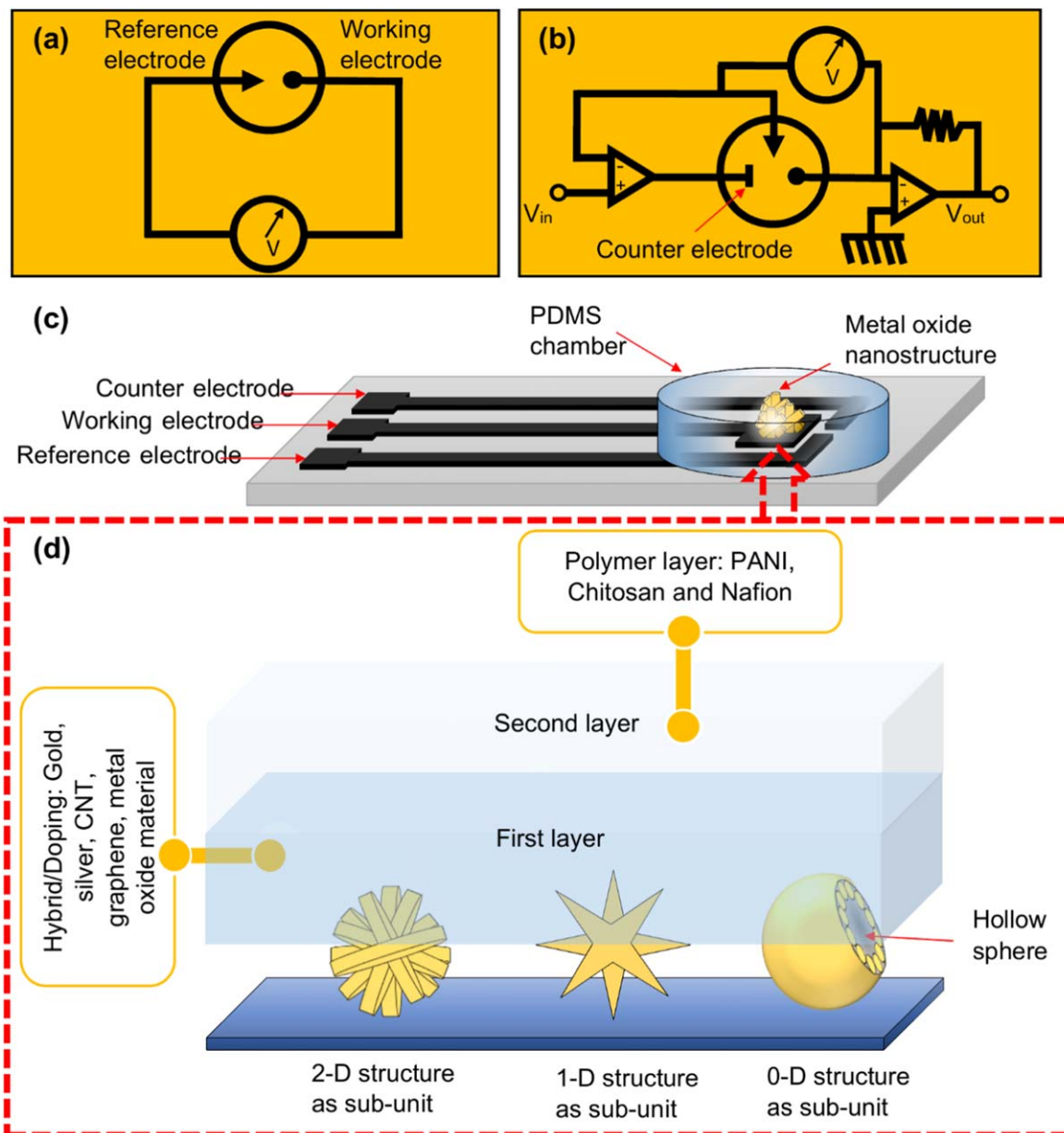


Figure 1. Basic circuit of (a) potentiometry (b) amperometry/voltammetry. (c) Schematic illustration of structure of nanostructured based electrochemical biosensor. And (d) the advance layer structure of 3-D ZnO as active site on working electrode.

This review aims to comprehensively report the synthesis route of 3-D ZnO via solution-based approaches together with promising advancements in current methods. Furthermore, the analytical performance of 3-D ZnO nanostructures-based electrochemical biosensors in detecting various biomolecules is reviewed with an emphasis on the use of nanocomposite materials, all of which are presented in three separate sections.

General Structure of Electrochemical Biosensors

Electrochemical biosensors are one of the transduction methods which transform the chemical reaction to electrical response to allow for quantitative analytical information. The electrode potential is given by the Nernst equation as²⁷;

$$E = E^0 - \frac{RT}{nF} \ln \left(\frac{Red}{Ox} \right) \quad [1]$$

Where E is the electromotive force, E^0 is the constant potential contribution to the cell, R is the universal gas constant, T is the absolute temperature in degrees Kelvin, n is the charge number of the electrode reaction, F is the Faraday constant, and Red and Ox is the chemical activity of reduced and oxidised species. Basically, there are three types of transduction methods in an electrochemical biosensor, namely potentiometry, amperometry, and voltammetry. The direct determination of the analyte ion concentration using the Nernst equation is referred to as direct potentiometry.²⁸ Potentiometry selectivity is inherent, has a high dynamic range and a log relationship with concentration, and is typically operated at equilibrium.^{29,30} The cell potential is measured at equilibrium. Changes in the cell potential must be solely due to changes in the working electrode potential. The reference electrode is typically a scarcely soluble salt film on metal such as Ag/AgCl/KCl and Hg/Hg₂Cl₂/KCl.^{27,31} Its role is to fix the potential difference between the conduction band and the solution.²⁷

For amperometry and voltammetry analytical methods, the voltage or the voltage programme is applied to the reference electrode. The current flows between the counter electrode and the working electrode, usually at virtue earth. The current and the current-voltage relationship are controlled by the redox reaction occurring at the working electrode.³⁰ The counter electrode must be large and inert. Typically, the current is measured at a constant potential referred to as amperometry. Current measured during controlled variations of the potential is referred to as voltammetry. The activity of the recognition element varies before and after interacting with the target molecule. The product must be electro-active and must undergo a redox process.³² Since not all protein analytes can serve as redox partners in electrochemical reactions, these devices mostly use mediated electrochemistry to facilitate the electrochemical reaction of the analyte at the working electrode.³³

3-D ZnO based electrochemical biosensor.—The 3-D ZnO is built via the agglomeration of tremendously low-dimensional nanostructures. The low-dimensional nanostructure consists of zero-dimensional (nanoparticles & quantum dots),³⁴ one-dimensional (nanofiber, nanotubes, nanorods, and nanowires),³⁵ and two-dimensional nanostructures (nanodisks, nanosheets and nanoflakes).^{36,37} The 3-D ZnO is usually larger than 100 nm but its sub-unit structure is in nanoscale.³⁸ The agglomeration of these low-dimensional nanostructures produces a variety of 3-D ZnO morphologies. For example, the aggregation of nanoparticles produces a microsphere and a hollow sphere.³⁹ The 1-D nanostructure turns into a nanoflower, or a tetrapod, and normally morphs into a spherical shape.^{40,41} Similarly, the 2-D nanostructure combines into a nanoflower, a lamellar shape, and a nanorose.⁴² All these morphologies are illustrated in Fig. 2. So far, review articles have extensively reported the 1-D and 2-D ZnO for biosensor applications but not the 3-D ZnO.^{43,44}

The 3-D ZnO has been employed in the construction of semiconductor-based sensing systems in medical diagnosis, to execute two main roles: as a mediator and to provide immobilisation support for bioreceptors.⁴⁵ The 3-D ZnO can facilitate the electron transfer rate between the transducer electrode and biological molecules. Furthermore, a good biosensor must have an ideal immobilisation platform. These two special roles of 3-D ZnO are strongly dependent on the size, novelty pore effect, and crystal defect of ZnO.^{41,46} The

3-D ZnO provides extra surface area due to its increased geometric volume; thus it is a better platform for immobilising bioreceptors. Furthermore, the unique property of its subunits and size enables it to achieve a synergic advantage during sensing measurements. Further advances can be achieved by tuning the electronic ability of 3-D ZnO-based electrochemical biosensors through the production of hybrid/doping nanomaterials with noble metals,^{47,48} carbon nanotube,⁴⁹ graphene⁵⁰ and metal oxide materials.^{51–53} Experimental and analytical modelling has shown that hybrid/doping concentration affects biosensing sensitivity.^{54,55} Some issues around enzyme leakage and a poor immobilisation process have necessitated the use of polyaniline (PANI), nafion, and chitosan for hybridisation with 3-D ZnO.⁵⁶

The 3-D ZnO Preparation based on Solution Approach

Different from other ZnO dimensional nanostructures, the synthesis methods of 3-D ZnO are quite limited. Several methods have been developed to synthesize the nanoparticles,⁵⁷ nanorods,⁵⁸ nanotubes,⁵⁹ nanowires,⁶⁰ nanosheets,⁶¹ and nanoflakes⁶² based on various techniques approaches such as vapour, solid, and solution. However, from the literature survey, solution approach is often used to synthesize 3-D ZnO because it can allow the self-assembly of the heterostructures or hybrid nanomaterials cost-effectively. Moreover, no additional template materials are needed to obtain the 3-D structure.⁶³ The solution approach includes hydrothermal/solvothermal, microemulsion, water bath, microwave-assisted, and electrodeposition methods have been found the most efficient for forming crystalline 3-D ZnO.⁴² Hydrothermal method is the process which is precursor solution is reacted in a closed system under controlled temperature and pressure with water as the solvent.⁶⁴ This conventional method have been widely used because of simple, cost effective and experimentally proved to fabricate all type of dimensionalities of ZnO.⁶⁵ Recently, another strategies proposed by using electromagnetic radiation via microwave method can enhance the crystallization kinetics in a short period.⁶⁶ Thus, the microwave method has exhibited excellent performance, successfully growing 3-D ZnO in a fast reaction time of 2–15 min.⁶⁶ This result is the best achievement in the literature so far. Nevertheless, each method has its advantages and disadvantages, as summarised by Wang et al.¹⁵ Nowadays, other studies have tried to hybridise two or more methods such as by combining the hydrothermal-electrodeposited methods⁶⁷ and

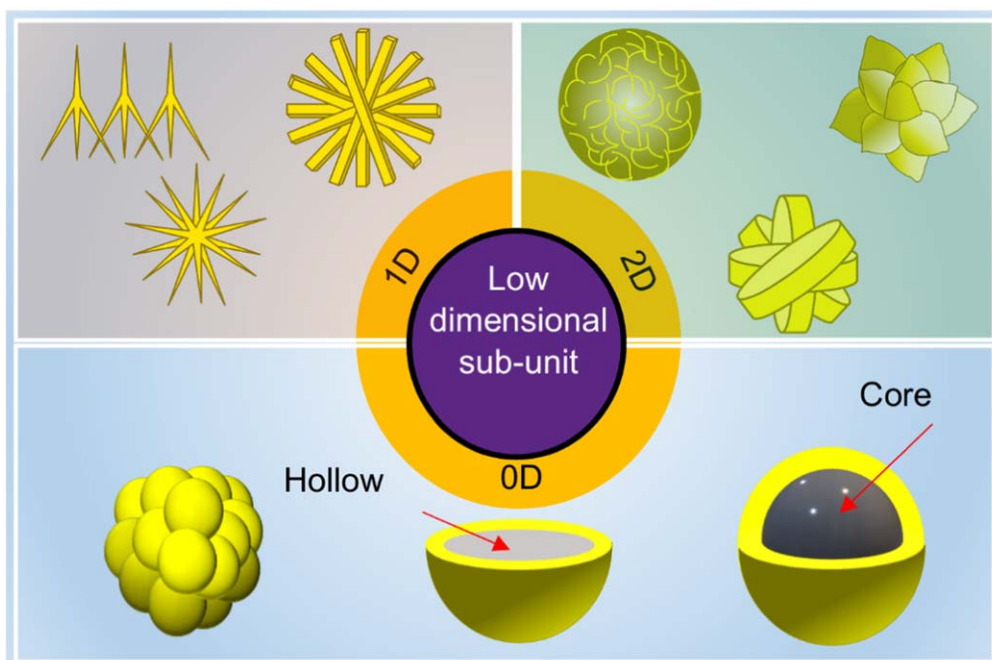


Figure 2. Various morphologies of 3-D ZnO nanostructures built based on low dimensional nanostructures such as zero dimensional (0-D), one dimensional (1-D) and two dimensional (2-D).

Table I. Overview of selected solution approaches for synthesising 3-D ZnO.

Morphology	Chemical precursor	3-D Technique condition
Nanoflower ⁶⁹	ZNH, N(II)NH, NaOH	Hydrothermal: 120 °C for 6 h
Nanoflower ⁷⁰	ZNH, TCD, NaOH	Aqueous solution route: stirring for 2 h, and dried at 60 °C for 12 h
Spherical nanorod ⁶⁶	ZNH, HMT, AH	Microwave: 10–15 min
Whisker-like ¹⁴	ZAD, NaOH	Water bath: 6 h at 65 °C
Spherical nanorod ⁷¹	ZNH, HMT	Hydrothermal: 90 °C for 4 h
Spherical nanorod ⁷²	ZNH, SNA	Hydrothermal: 150 °C for 5 h
Nanopetal hexagonal ⁷³	ZCl, AH	Water bath: 90 °C for 4 h
Triangular petal ⁷⁴	ZNH, SN, AH	Hydrothermal: 150 °C for 5 h
Spherical nanowire ⁷⁵	ZNH, HMT, AH, PEI	Hydrothermal: 90 °C for 24 h
Hollow sphere ⁷⁶	ZNH, D-Glucose, urea	Hydrothermal: 180 °C for 20 h and post annealing: 500/600 °C for 4 h
Hollow sphere ⁷⁷	ZNH, D-Glucose	Hydrothermal: 180 °C for 20 h and post annealing: 270–550 °C for 3 h
Hollow sphere ⁷⁸	ZNH, D-Glucose, C(II)N	Hydrothermal: 180 °C for 24 h
Hollow sphere ⁷⁹	ZNH, HMT, AH, TCD	Reflux condenser: 80 °C for 1 h
Nanoflower ⁸⁰	ZAD, AH, NaOH	Sonochemical: 57 °C–70 °C for 30–60 min

Abbreviation: ZNH: Zinc nitrate hexahydrate, TCD: Trisodium citrate dihydrate, ZAD: Zinc acetate dihydrate, AH: Ammonia hydroxide, ZCl: Zinc chloride, SNA: Silver nitrate ammonia, HMT: Hexamethylenetetramine, PEI: Polyethyleneimine, N(II)NH: Nickel (II) nitrate hexahydrate, D-Glucose: Glucose monohydrate, NaOH: Sodium hydroxide, C(II)N: Copper (II) nitrate.

microwave assisted hydrothermal methods.⁶⁸ The various synthesis conditions used to fabricate 3-D ZnO using solution approaches are summarised in Table I. There are two different technique to grow 3-D ZnO on substrate. First technique is to grow directly on a substrate. Second technique requires the 3-D ZnO to be synthesised separately in other medium before being coated or transferred to a substrate.

There are similar growth mechanisms and key parameters in the formation of 3-D ZnO. As the hydrothermal method is the most popular, this section outlines it as a flagship method. Typically, in a bottom up technique, two steps of the process have been widely used in the literature. The first step is to prepare a seed layer. This seed layer will provide active sites and minimise surface energy for the 3-D ZnO to attach to it. The second step is to prepare the second layer (3-D structure) using the hydrothermal method. A schematic summary of the hydrothermal method is given in Fig. 3a.

Figures 3b and 3c show the growth mechanism of wurtzite structure of 3-D ZnO, which normally occurs in a precursor solution. At the early stage, hydroxyl ions are released from the OH[−] source, which reacts with Zn²⁺ ions to form a Zn(OH)₄^{2−} complex (Step 1). The self-assembly process between the complex cluster via a kinetic driving force subsequently leads to the formation of ZnO nuclei (Step 2).⁸² Then, the smaller particles are consumed by the larger particles so that the ZnO nuclei merge into ZnO crystallites, also known as the Ostwald ripening effect (Step 3). Under low surface energy, these crystalline structures provide active sites to facilitate directional growth in the [0001] orientation (*c*-axis). A large number of low-dimensional nanostructures then forms 3-D ZnO structures (Step 4) until it gains weight and bonds with the seed layer.

Conventional methods have undergone advances and modifications in the past few years. One of the research trends nowadays includes the narrowing of the conventional method to involve only eco-friendly materials in the precursor solution preparation. For example, acetone is an organic solvent that can replace the additive stabiliser normally used in conventional methods, such as triethylamine (TEA), which harms the environment.⁸³ Many studies have reported about using of plant and microorganism components to prepare the precursor solution.⁸⁴ For example, the bio-extract of Avocado fruit, aloe Vera, and citrus contains free radicals such as superoxide anions and hydroxyls.^{85,86} These reactive oxygen species are capable of adsorbing electrons from surrounding molecules and reacting with zinc ions. They also act as reducing and stabilising agents for the synthesised nanostructures.⁸⁷ Another studies have used microorganisms such as *Chlamydomonas reinhardtii*⁸⁸ and *Sargassum muticum*⁸⁹ to stabilise the zinc nanostructure. The amino groups in the microorganism protein can adsorb onto the negative polar surface of ZnO via hydrogen bonding.⁸⁸ This reaction results in rapid growth along a positive polar (0001) plane; thus

forming nanorods that are then agglomerated into a spherical shape.⁸⁸ To the best of the author's knowledge, this method only focuses on antimicrobial activity applications. No study has yet used the bio extract of plants, nor have any involved a microorganism in the fabrication of nanostructure-based biosensing devices. So far, this eco-friendly material is a promising approach that offers a safe route for preparing 3-D nanostructure-based biosensors.

Another advancement in the conventional method is the use of a patterned substrate to control the positioning of the 3-D ZnO on the substrate. This can be categorised as a top-down technique, which usually uses a lithography step to accurately align the desired array of 3-D ZnO on the substrate.^{81,90} However, this method cannot achieve as good a downscaling result as the bottom-up approach. The conventional electro-beam lithography and photolithography as one part for this technique.⁹¹ Nowadays, nanoimprinted, colloidal, soft, and dip-pen lithography is also known as part of the novel lithography process.⁴⁴

Synthesis parameter.—The physicochemical properties of ZnO nanostructures are known to be highly dependent on the size and morphology of the ZnO. Therefore, to generate effective size distribution and morphologies, it is necessary to optimise both the cultural condition and the varied physical parameters of the ZnO synthesis process, including pH, temperature, precursor concentration, type of precursor element, and reaction time. Every parameter is inter-related. There is also a never-ending debate on realising the potential function of each parameter, as all parameters depend on each other. However, the literature shows that the five major parameters in hydrothermal process are reaction time, hydrothermal temperature, precursor concentration, the pH of the precursor solution, and the precursor type.^{92,93}

Reaction time.—Reaction time has a vital role in increasing the length and grain size of 3-D ZnO nanostructures.⁹⁴ Starting from the nucleation process that needs a certain period of time followed by the crystal growth process. This crystallization process will occur at a faster rate at higher reaction time and may result in increased of nanostructures size. The 3-D ZnO nanostructures continuously gain their size until it reaches a maximum length and Zn²⁺ ion in precursor solution is reduced.⁹⁵ However, re-nucleation process will take place when the reaction time is prolonged further. This indicates the 3-D morphology of ZnO can be tailored as proved by Agarwar et al.⁹⁶ Besides, Molefe et al.,⁹⁷ who synthesised ZnO nanostructures using chemical bath deposition, indicated a decrease in the energy band-gap with increased reaction time.

Temperature.—Feng et al.⁹⁸ found that the nucleation and crystal growth of ZnO is highly dependent on temperature. High temperatures

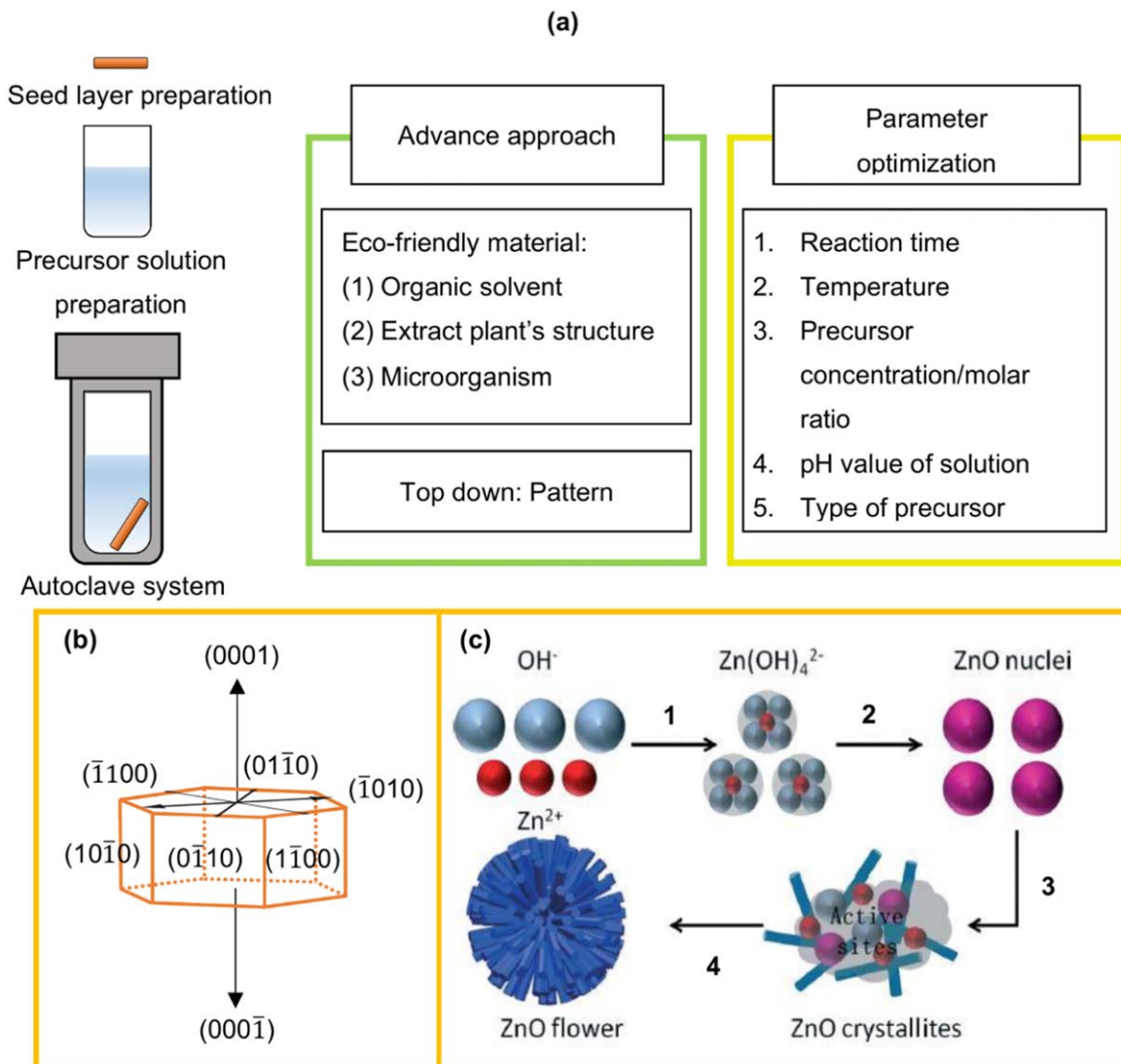


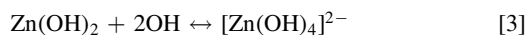
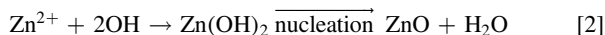
Figure 3. (a) The hydrothermal preparation of 3-D ZnO using an advanced approach and key parameters; (b) a crystal structure model of wurtzite ZnO; and (c) a schematic mechanism of the 3-D ZnO growth formation. (Fig. 3c is reproduced with permission from Ref. 81 © Royal Society of Chemistry 2015).

made the nuclei sites in the solution more prone to agglomerate into a 3-D formation. The rate of the nucleation was higher than the crystal grain growth when a low temperature was used. With a temperature increase, the crystal grain growth was greatly facilitated, and it was easier for the grain that formed to aggregate together. These findings are consistent with those of previous studies, which found that the synthesis of ZnO in solution could be explained according to two steps. First, low temperatures favour the growth of homogeneous rod, and second, high temperatures induced competition between growth and nucleation.^{99,100}

Precursor concentration.—Another key factor that influences the density and the average diameter of subunits of 3-D ZnO is precursor concentration. The concentration of the growth solution (i.e., the concentration of Zn²⁺ and OH⁻) is crucial to the formation of the Zn(OH)₄²⁻ precursor and hence controls the nucleation rate.⁷⁵ The diameter of the subunit, especially that of the nanorods or nanowires in the 3-D ZnO structures, uniformly increase with increasing solution concentration. Thus, it is best to use a low concentration precursor to obtain 1-D nanostructures with a high aspect ratio as the subunits of 3-D ZnO. This result is similar to that of another finding.⁷¹

The pH value of precursor solution.—On the other hand, when the OH⁻ ions are more than the Zn²⁺ ions, the OH⁻ not only

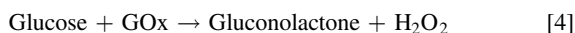
becomes a source of hydroxyl ions for forming ZnO but also acts as a capping agent.¹⁰¹ Therefore, the pH of the solution (depend on amount of OH⁻ ions) is another key factor that influences ZnO morphology. The ZnO crystal is a polar solid with a positive polar plane (0001) rich in Zn and a negative polar plane (000 $\bar{1}$) rich in O.¹⁰² The OH⁻ ions are preferably adsorbed onto the (0001) plane of ZnO. This condition suggests that the OH⁻ ions can act as a surface termination reagent, thus impeding the growth of the crystal face (0001). Furthermore, the amount of OH⁻ concentration in the precursor will significantly influenced their (ZnO) growth species unit. The formation of 3-D ZnO nanostructures will follow two possible chemical reactions, as per Eqs. 2 and 3. Normally, Eq. 2 indicated how nucleation process occur for equalmolar of Zn²⁺ and OH⁻ in solution. Thus an initial morphology of 3-D ZnO is formed. Then, further increase of OH⁻ would promote the Eq. 3, the [(Zn(OH)₄]²⁻ complex to be the new growth species. While in Eq. 2, the complex will serve as a seed layer for tuning the morphology of 3-D ZnO into a new form.¹⁰³ As in another work found that, further increases in pH would result in a fast reaction that follows a nucleation-dominated process, leading to the formation of spherical nanoparticles.¹⁰³ In addition, the subunit morphology 3-D ZnO morphology of ZnO can be modified by using different pH value of precursor solution which can be found in previous works by Kim et al.¹⁰⁴ and Yi et al.¹⁰⁵



Type of precursor.—The type of precursor also plays an important role in tailoring the morphology of the ZnO nanostructures. Several works have shown the influence of zinc precursors on the ZnO morphology and particle size. Zinc nitrate and zinc acetate stand out from other zinc sources that are commonly used in the hydrothermal approach because of their higher solubility in organic solvents.¹⁰⁶ Moreover, it has been shown that introducing any growth modifiers (for example, capping ligands), which have a specific affinity towards any crystal face of surface, can modify the relative growth rates of ZnO—reflected in the final crystal shape.¹⁰⁶ Many studies have investigated the effect of capping agents/different soft templates (surfactants, polymers, di-block copolymers, citric acid, ascorbic acid and amino acids).¹⁰⁷ However, by understanding in-depth, the influence of each of these parameters, optimum conditions can be achieved to produce 3-D ZnO structures that can meet the required application.

Sensing Application for Different Biomolecules

Glucose, hydrogen peroxide and cholesterol.—The ZnO nanostructure-based electrochemical biosensors are already extensively used to detect glucose. The fast and accurate determination of glucose using this method has profound applications since glucose concentration is a crucial indicator of many diseases such as diabetes and endocrine and metabolic disorders. In this section, hydrogen peroxide is touched on in detail, as it is one of the by-products of glucose oxidation catalysed by glucose oxidase (GOx) in the presence of O₂; the detection of glucose can be achieved based on monitoring the production of H₂O₂, as per Eq. 4.¹⁰⁸ The morphology of 3-D ZnO will influence its sensing performance especially during immobilisation of the bioreceptor.



Previously, Fang et al. found that a smooth surface such as that of ZnO nanoflowers was not beneficial for immobilising GOx.¹⁰⁹ Thus, they proposed using ZnO hollow nanospheres, which have efficient adsorbing properties and a pore effect, a low density, and better direct electron transfer for immobilising GOx. The pore effect can maintain enzyme activity, as its geometric volume can increase the probability of GOx to keep in contact with the semiconductor surface—either the

GOx stays in or outside the pores. As a result, the sensitivity measured for ZnO hollow nanospheres ($65.82 \mu\text{A mM}^{-1} \text{cm}^{-2}$) was higher than that of ZnO nanoflowers ($41.13 \mu\text{A mM}^{-1} \text{cm}^{-2}$). The ZnO hollow nanospheres also had a lower limit of detection ($1.0 \mu\text{M}$) compared to the ZnO nanoflowers ($3 \mu\text{M}$). Rafiq et al.¹¹⁰ conducted a further study and found that the formation of ZnO microspheres with numerous pores caused them to have a high specific surface area and were therefore desirable as fillers for GOx enzyme loading. The Barrett-Joyner-Halenda (BJH) model was used to further investigate the pore volume of ZnO after the nanostructure has been analysed using N₂ adsorption-desorption isotherms. Based on its sensing performance, the high specific surface area of the ZnO microspheres not only improved protein/enzyme immobilisation efficiency but also enhanced the charge transport and sensing performance.¹¹⁰ Tripathy et al.¹¹¹ also used ZnO hollow spheres to detect cholesterol. They proposed a low-temperature solution preparation to fabricate hollow nanosphere-based cholesterol biosensors. The result was a product that was mixed with butylcarbitol acetate before being cast onto a sputtered Ag/glass electrode. This approach successfully synthesised well-distributed porous nanospheres with an average pore diameter of 4.1 nm. The fabricated device exhibited a low limit of detection (0.4 mM) with a wide linear detection range ($0.2\text{--}15.6 \text{ mM}$), a fast response time (2 s), and high sensitivity ($99.8 \text{ mA mM}^{-1} \text{cm}^{-2}$). The device also showed good accuracy after being tested on a human serum sample.

Recently, Zhou et al. demonstrated a different morphology of 3-D ZnO, which is a micro-pompon structure, for H₂O₂ detection.¹¹² The study fabricated ZnO micro-pompoms by controlling a synthesis route via a soft template-directed wet chemical method, subsequently annealed in ambient air. The prepared ZnO micro-pompoms (Fig. 4a) was a few hundred micrometres in diameter and composed of a great amount of robust 1-D nanostructures (Fig. 4b) built of numerous 0-D nanostructures (Fig. 4c). This unique low-density structure provided a large space between the 1-D nanostructures, making it accessible for the mobilisation of analytes. Furthermore, the flow of electrons was also facilitated, resulting in tightly-connected nanoparticles. Subsequently, horseradish peroxidase was immobilised on the ZnO micro-pompoms and then its outside covered with chitosan. A wide linear range of $0.2\text{--}0.34 \text{ mM}$ and high sensitivity of $1395.64 \mu\text{A mM}^{-1} \text{cm}^{-2}$ were also recorded, indicating excellent H₂O₂ sensing performance.

The unique morphological structure of 3-D ZnO promises great potential for enhanced detection performance of glucose, H₂O₂, and cholesterol. However, an insulating effect occurs between the redox proteins and the electrode supports, which is a key factor that limits the development of these biosensors. For example, the redox centre of GOx, which is flavin adenine dinucleotide (FAD), is responsible

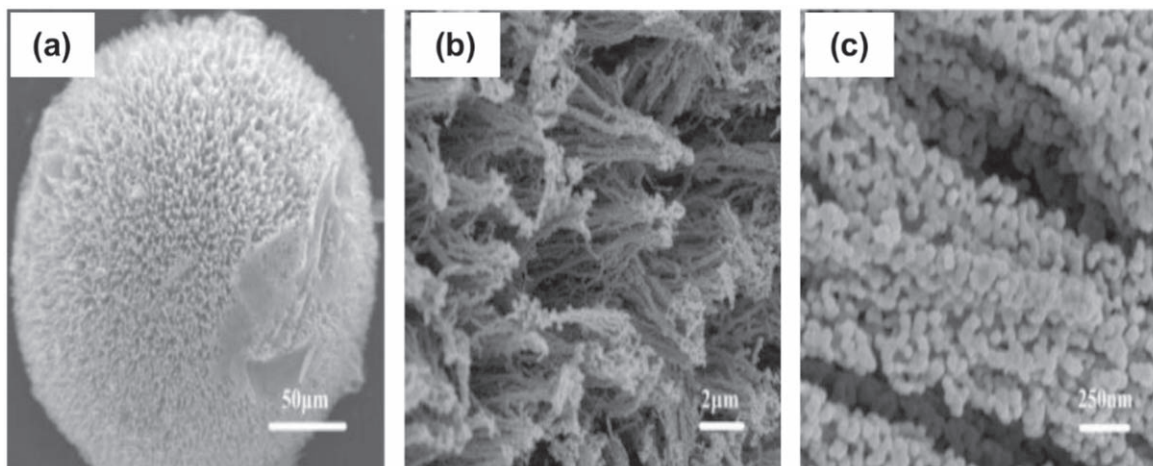


Figure 4. SEM images of (a) 3-D ZnO micro-pompoms with $50 \mu\text{m}$ of scale bar, consist of (b) nanowire with $2 \mu\text{m}$ of scale bar and built of (c) nanoparticles with 250 nm of scale bar (reprinted with permission from Ref. 112, © Elsevier 2014).

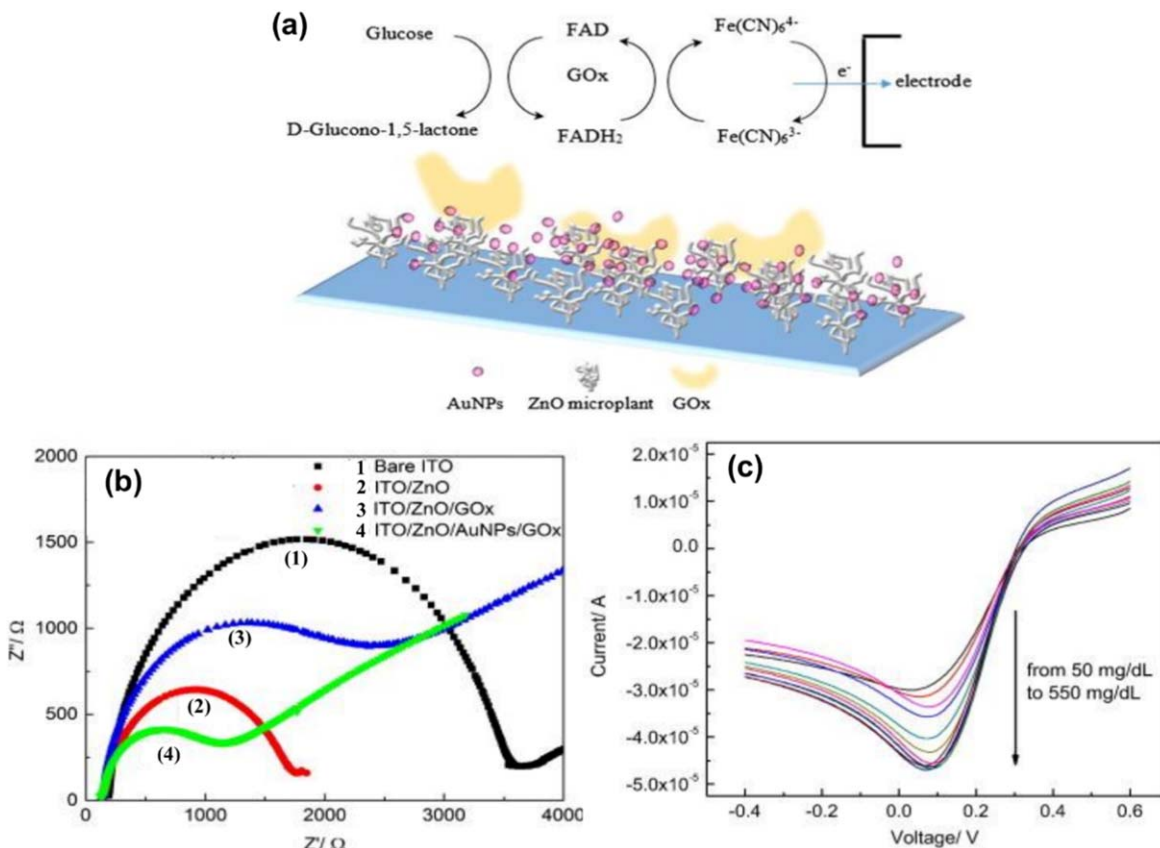


Figure 5. (a) The electrochemical reaction at the ZnO/AuNP/GOx/ITO electrode and the scheme of the prepared sensor based on ZnO/AuNP/GOx/ITO; (b) the EIS plot of the different layer-based bioelectrode; (1) bare ITO; (2) ITO/ZnO; (3) ITO/ZnO/GOx; and (4) ITO/ZnO/AuNP/GOx, respectively, in PBS solution from 0.1 Hz to 10^5 Hz at 100 mV; (c) the plot of LSV of ITO/ZnO/AuNPs/GOx with different glucose concentrations (reprinted with permission from Ref. 115, © Elsevier 2015).

for catalysing the glucose during oxidation reactions. However, this redox centre is covered with a thick protective protein shell that blocks the electron transfer process.^{113,114}

To overcome this issue, Tian et al.¹¹⁵ used gold nanoparticles (AuNPs) to attach uniformly onto ZnO microplants, as illustrated in Fig. 5a. The AuNPs has a similar role to that of FAD in enzyme system and provides a more active surface for FAD; thus, improving the transfer of electrons across the GOx along the biosensor layer structure. Enhanced electrical transport was clearly observed based on the change in the charge transfer resistance (R_{ct}) on the Nyquist plot, as shown in Fig. 5b. The large semicircle diameter on the Nyquist plot represents a high R_{ct} value for the electrode. Figure 5b–1 indicates the bare ITO electrode exhibiting poor electron transfer, as it possesses a high R_{ct} . However, depositing ZnO microplants onto the bare ITO electrode reduced the value of R_{ct} (Fig. 5b–2). Then, loading the GOx onto the ZnO/ITO resulted in an increase in the semicircle size (Fig. 5b–3) due to an insulating effect, as the enzyme protein blocked the charge transfer process. The electrical properties greatly improved the sample ITO/ZnO/AuNPs/GOx. The Nyquist plot for the sample in Fig. 5b–4 showed the smallest semicircle diameter, indicating the lowest value of R_{ct} (1238 Ω) compared to all other samples. The study also found a lower value of the Michaelis Menten constant (K_m) for the GOx immobilised on the electrode (1.70 mM) using the Lineweaver-Bruke equation, which reflects the increasing activity between the enzyme and the electrode. When the active site of the biosensor interacted with a glucose concentration ranging from 50 mg dl⁻¹ to 400 mg dl⁻¹, the current changed linearly during the linear sweep voltammetry (LSV) measurement (Fig. 5c). However, above concentrations of 400 mg dl⁻¹, the linear increases reduced, possibly due to the saturation of glucose molecules on the electrode surface or the

limited catalytic activity of glucose oxidase. In the end, the sensitivity was determined to be 3.12 $\mu\text{A mM}^{-1} \text{cm}^{-2}$ in the linear range of 50 mg dl⁻¹ to 400 mg dl⁻¹.

Many research groups such as that of Fang et al.¹¹⁶ and Hussain et al.¹¹⁷ have demonstrated the noble metal hybridisation of 3-D ZnO nanostructures to detect glucose molecules at low concentration. The functionalisation of 3-D ZnO nanostructures with AuNPs (noble metal) may also be of considerable interest in the development of high-performing semiconductor biomedical devices. Not only that, but it also shows great promise as a biosensing platform for glucose detection.¹¹⁶ Despite the unique advantages of 3-D ZnO nanostructures, they are still not recommended for fabricating enzyme-free biosensors—unlike the low-dimensional ZnO structures, especially ZnO nanowires and nanorods, which have become primary candidates for enzyme-free biosensors.^{60,118} The non-enzymatic or enzyme-free biosensor is the fourth generation biosensor. These biosensors can solve the problem faced by enzymatic biosensors such as poor stability, high time-consumption for immobilising the enzyme, and an expensive preparation for the enzyme. Therefore, the development of enzyme-free 3-D ZnO-based biosensors must also be looked into in more detail.

Dopamine, Levodopa, uric acid and ascorbic acid.—A recent discovery that dopamine (DA), levodopa (LD), uric acid (UA), and ascorbic acid (AA) can cause serious neurological disorders has been attracting intense attention from various fields of research. Parkinson's disease and Schizophrenia are one of the negative effects of a deficiency of DA in the brain.¹¹⁹ Meanwhile, LD has been chosen as an immediate precursor to DA. It possesses the ability to penetrate a semipermeable membrane, such as the blood-brain barrier, and can then transform itself into DA via enzymatic

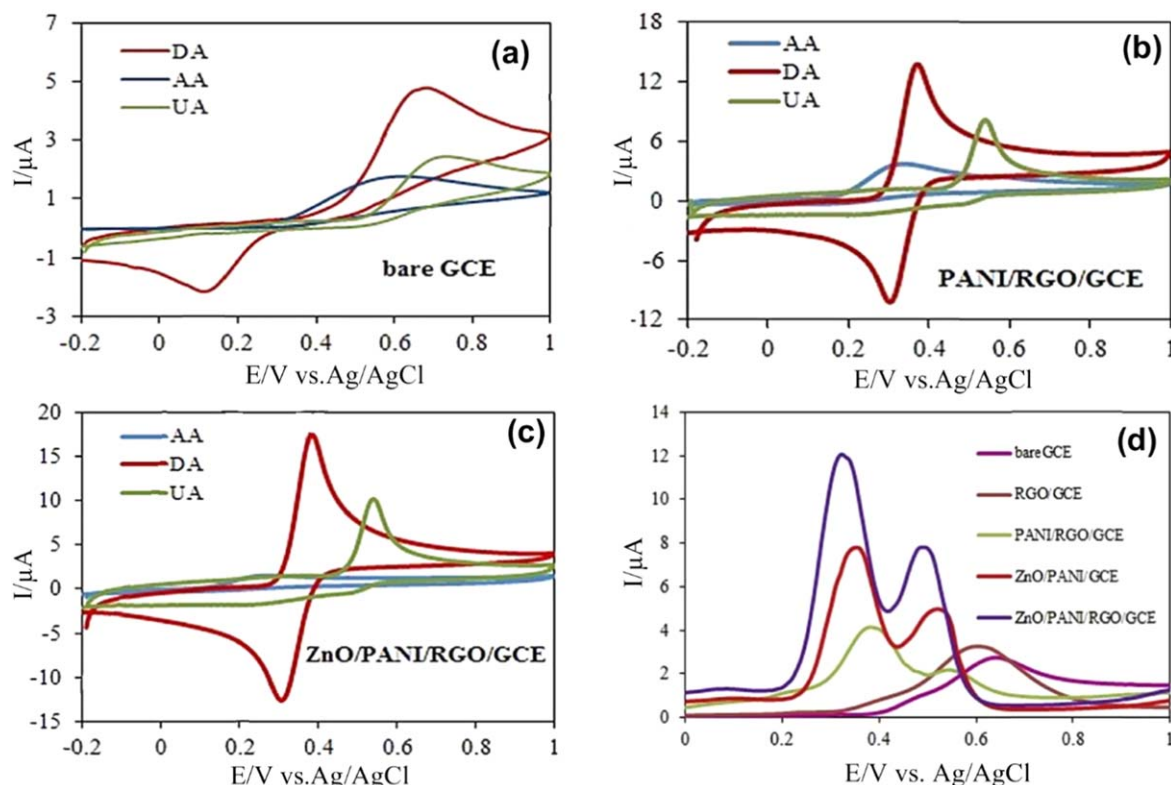


Figure 6. The cyclic voltammograms of 10 mM AA, 1.0 mM DA, and 10.0 mM UA at the (a) bare GCE, (b) PANI/RGO/GCE, and (c) ZnO/PANI/RGO/GCE in 0.1 MBR (pH 4.0) at a scan rate of 50 mV s^{-1} ; (d) DPVs of the mixture of 1.0 mM AA, 80 mM DA, and 800 mM UA in 0.1 MBR (pH 4.0) at different electrodes with a scan rate of 50 mV s^{-1} and a pulse amplitude of 25 mV (reprinted with permission from Ref. 130, © Elsevier 2016).

action.¹²⁰ However, high-level concentrations of LD can cause toxic metabolites to form via the auto-oxidation of the LD, which leads to several side effects such as vomiting, nausea, and dyskinesia.¹²¹ Another oxidative species is uric acid (UA), which is the metabolism product of urine. Patients suffering from hyperuricemia and the Lesch-Nyhan syndrome have abnormal concentrations of UA. On the other hand, ascorbic acid (AA) is an essential vitamin in the human body. It plays a vital role in the treatment and inhibition of infertility, the common cold, and mental illnesses.^{122,123} DA, UA, and AA coexist in the extracellular fluids of the central nervous system.^{124,125} Tremendous consideration has been given to designing selective and sensitive electrochemical biosensors for determining DA, with an urgent challenge to use an electrochemical method to sense DA under physiological conditions. The very low basal concentration of DA ($0.01\text{--}1.0 \mu\text{M}$)¹²⁶ can serve as an intensive barrier to other species such as AA and UA, which have much higher concentration levels (100–1000 or higher).¹²⁷ Furthermore, AA has nearly the same oxidation potential to that of DA at almost all solid electrodes; hence resulting in poor specificity and sensitivity in DA detection.¹²⁶

Recently, the 3-D ZnO nanostructures have been used as support nanocomposite materials for DA detection.¹²⁸ Then, Fang et al.¹²⁹ demonstrated the promise of 3-D ZnO nanostructures (nanosheets as the subunit) decorated with AuNPs to enhance current response. The study also investigated the effect of pH and the scan rate of cyclic voltammetry for optimising the conditions to determine DA.

Interestingly, Ghanbari and Moloudi successfully detected DA and UA simultaneously in the presence of AA using flower-like ZnO/Polyaniline/reduced graphene oxide nanocomposite-based electrochemical biosensors.¹³⁰ The electrochemically-reduced graphene oxide (RGO) is environmentally friendly and low-cost and has been used to hasten the sensing process. The presence of the conjugate polymer of polyaniline (PANI) in RGO reduces the aggregation of and stabilises the formation of RGO. Since PANI has low sensing

interaction and mechanical strength, it is necessary to composite it with the ZnO nanostructure. The nanocomposite has a high electronic interaction between metal oxides, PANI, and the graphene matrix, which increases the electron transfer rate of the material, as shown in Fig. 6, which indicates a cyclic voltammetry measurement of 10 mM AA, 1.0 mM DA, and 10.0 mM UA at three different electrodes in 0.1 MBR (pH 4.0) at a scan rate of 50 mV s^{-1} . When bare glassy carbon electrode (GCE) was used, the oxidation peak current for DA, UA, and AA was unclear (Fig. 6a). In contrast, Fig. 6b shows that the redox behaviour of DA, UA, and AA was greatly enhanced using the PANI/RGO/GCE electrode. Each electroactive species revealed a clear oxidation peak potential that was higher than the bare GCE electrode due to an increment in the active surface areas of the PANI/RGO. The ZnO/PANI/RGO/GCE indicated a high specificity towards DA and UA, as each of their oxidation peaks current was observed and defined without an interference peak from AA, as shown in Fig. 6c. Then, the differential pulse voltammetry method was applied to improve the oxidation peak current of the three electroactive species individually. This analytical method was able to eliminate the non-Faradic current compared to the cyclic voltammetry method. As a result, the peak potentials from each species were well defined, as shown in Fig. 6d. This synergy in material between 3-D ZnO, graphene, and the PANI nanocomposite produced a large active surface area, with an efficient adsorptive capability of the nanomaterials and a high selectivity towards DA and UA. The linear range recorded for DA was $0.1\text{--}90 \mu\text{M}$ and $90\text{--}1000 \mu\text{M}$ with a detection limit of $0.017 \mu\text{M}$. For UA, its linear range was $0.5\text{--}90 \mu\text{M}$ and $100\text{--}1000 \mu\text{M}$ with a detection limit of $0.12 \mu\text{M}$.

Recently, Huang et al. demonstrated double 3-D nanomaterials consisting of ZnO nanosheet balls and highly conductive graphene foam without defect and junction resistance for DA determination.¹³¹ They used nickel foam as a template to grow the graphene foam (GF) based on chemical vapour deposition. Then, hydrothermal ZnO

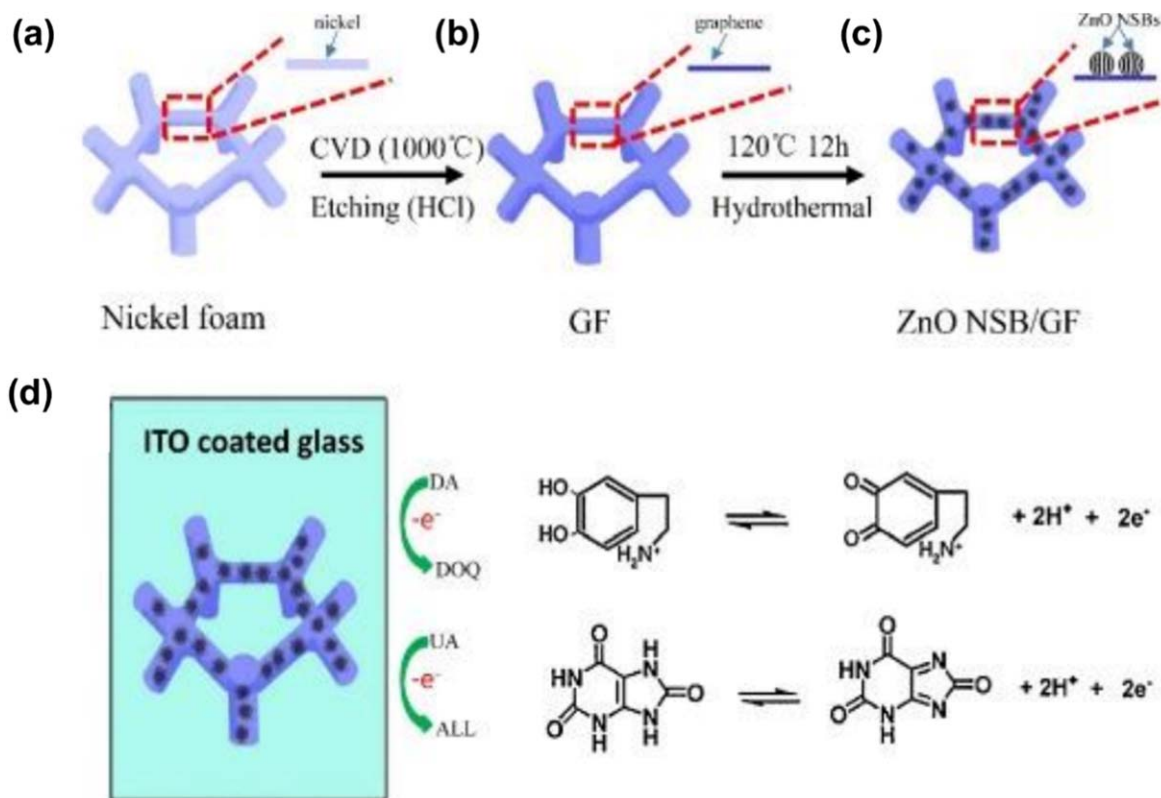


Figure 7. A schematic of the preparation process of ZnO nanosheet balls/GF and the electrochemical redox reactions of DA and UA at the ZnO nanosheet balls/GF electrode; (a)–(b) the graphene is deposited using CVD on the surface of the nickel foam and etched with HCl to get GF; (c) the hydrothermal process for depositing ZnO nanosheet balls on the GF surface; (d) the electrochemical redox reactions of DA and UA biomolecules at the ZnO nanosheet balls/GF electrode (reprinted with permission from Ref. 131, © Elsevier 2018).

nanosheet balls were distributed on the GF. The schematic procedure of the ZnO nanosheet balls/GF nanocomposite is illustrated in Figs. 7a–7d. The as-prepared ZnO nanosheet balls with a diameter of $\sim 2 \mu\text{m}$ and a sheet thickness of $\sim 50 \text{ nm}$ showed a high sensitivity ($0.99 \mu\text{A } \mu\text{M}^{-1}$) toward DA. In another report, Yue et al.¹³² utilised a similar method for synthesising double 3-D nanomaterials consisting of 3-D ZnO and GF. The diameter and a sheet thickness of 3-D ZnO were $\sim 2 \mu\text{m}$ and $\sim 100 \text{ nm}$, respectively. Then, the device was employed for the determination of LD in the presence of UA. The oxidation peak potentials (CV measurement) of LD increased rapidly with increasing LD concentrations from $0 \mu\text{M}$ to $75 \mu\text{M}$. Yue et al. conducted another study to investigate the effect of reaction reagents on the size of ZnO nanoflowers.¹³³ In their fabrication process (hydrothermal), ammonium hydroxide added to the precursor solution reacted with zinc ions to form complexes and lowered the degree of the supersaturation of the reaction system. This situation potentially suppressed the homogeneous nucleation process of the 1-D structure (a subunit of the ZnO nanoflower). As a result, the ratio of the length and diameter of the ZnO nanoflowers were increased. Similarly, the polyethyleneimine (PEI), which can be adsorbed onto the surface of ZnO nanoflowers, experienced a further increase in the 1-D subunit aspect ratio. Thus, the study found that the optimum size for the length and diameter of the ZnO nanoflower for LD detection were $2.5 \mu\text{m}$ and 50 nm , respectively.

In 2018, Yue et al.¹³⁴ fabricated multilayer graphene with a surface-sculptured ZnO nanoflowers/ITO electrode to enhance the conductivity and retain the absorption of biomolecules. The nanostructure with a length of $\sim 2.5 \mu\text{m}$ and a diameter of $\sim 50 \text{ nm}$ produced high sensitivity ($0.32 \mu\text{A } \mu\text{M}^{-1}$) with a limit of detection of $1 \mu\text{M}$ for LD. Most recently, the same authors synthesised a nanocomposite material by dispersing $\sim 150 \text{ nm}$ diameter of ZnO nanoflowers with a graphene oxide nanosheet.¹³⁵ The material was coated onto an ITO substrate for electrochemical biosensing

operations. The sensor was functionalised with LD in a PBS solution (pH 7.4) and the sensitivity of the sensor was observed to be $0.66 \mu\text{A } \mu\text{M}^{-1}$, which is higher than their previous work.¹³⁴

Nucleic acid and infectious disease.—The DNA biosensors have been gaining substantial recognition in the field of disease diagnostics since 1993.¹³⁶ Almost all infectious bacteria are made up of protein. Nowadays, our technology enables us to extract and customise a single-strand DNA (ssDNA) of bacteria to be used as a probe. Since then, the rapid and highly selective determination of various gene-based ZnO-based electrochemical biosensors have been documented, especially in the detection of dangerous diseases such as the chikungunya virus,¹³⁷ dengue,¹³⁸ breast cancer,¹³⁹ tuberculosis,¹⁴⁰ leptospirosis,⁴¹ the human immunodeficiency virus,¹⁴¹ and lung cancer.¹⁴²

These biosensors mainly work based on the principle of DNA recognition—by immobilising a single-strand DNA as a probe on a transducer active area and subsequently hybridising the target DNA to form a double-helix DNA. This DNA recognition could be hybridised onto ZnO nanostructures to generate an electrical signal. The preparation of a DNA recognition interface is the most crucial process in synthesising an electrochemical DNA biosensor. Besides, the immobilisation method for the DNA probe onto the ZnO surface also affects the performance of the biosensor in terms of sensitivity, selectivity, lifespan, and accuracy.

There are two popular approaches for immobilising DNA onto a ZnO surface. The first is physical adsorption, which is based on two different charge interactions. Under a neutral physiological surrounding (pH = 7), the ZnO nanostructures (IEP 9.5) exhibit a positive charge whereas the DNA (IEP 4.2) is negatively charged.¹⁴³ This condition makes it possible to immobilise the DNA onto the ZnO surface via electrostatic interaction. The second is via covalent bonding, which is based on chemical bonding. Figure 8 briefly compares these two approaches for immobilising ssDNA with the

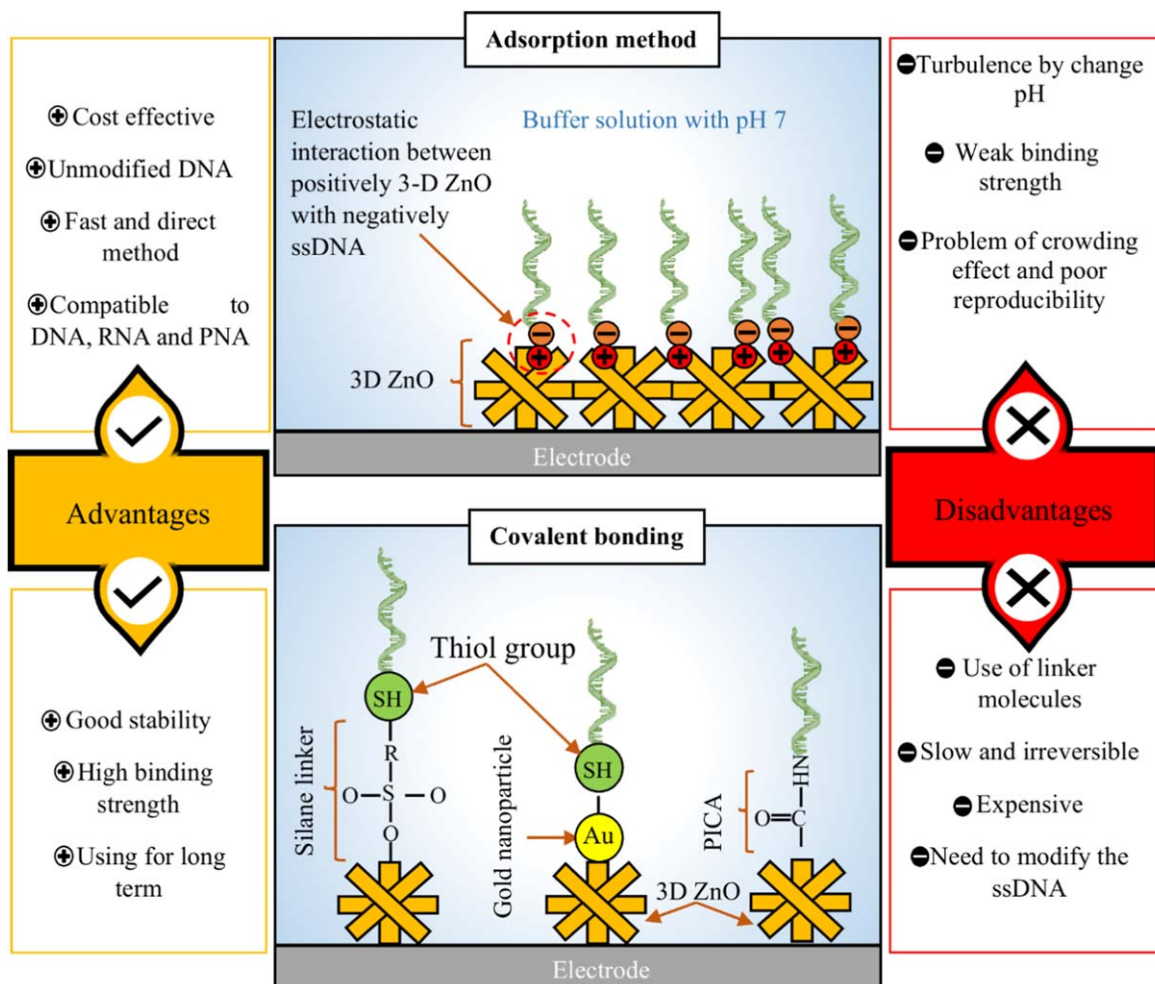


Figure 8. Comparison between physical adsorption and covalent bonding of DNA immobilisation on 3-D ZnO nanostructures with their advantages and disadvantages.

3-D ZnO nanostructures. A detailed review of the DNA immobilisation process onto different materials can be referred to in Rashid and Yusof.¹⁴³

Meningitis is one of the infectious diseases caused by bacteria that can lead to brain damage. Previously, a gold electrode was used for the detection of meningitis, but this method caused a lot of problems such as a low detection range, less sensitivity, and poor loading hybridisation.^{144,145} Until 2014, Tak et al.¹⁴⁶ demonstrated that ZnO nanoflowers (ZnONFs) could be effectively functionalised with an ssDNA sequence of *N. meningitis*. The ZnONFs were made from the agglomeration of nanorods and possessed an average length of 2.5 μm and a diameter of 100 nm. The topography and size of the ZnONFs were the main factors that caused the maximum loading of ssDNA. After calculating the surface concentration of the adsorbed species over the surface of the transducer-based on the Brown-Anson model,¹⁴⁷ better immobilisation efficiency was achieved compared to that of Lui et al.¹⁴⁸

Another approach indicating DNA hybrid efficiency was done using noncovalently binding ligands of a methylene blue (MB) mix in the concentration of the complementary target DNA. Via semi-intercalation and electrostatic binding, the MB molecules were able to attach themselves to the unpaired nitrogenous bases present in the ssDNA.¹⁴⁹ Hence, in the DPV signal, the peak oxidation current was higher when a large number of MB molecules bonded with the ssDNA due to the higher availability of the unpaired nitrogenous bases. Reducing the availability of the unpaired bases due to the hybridisation of the probe ssDNA with the target DNA resulted in a lesser association of the MB molecules. As a result, a lower value of

the peak oxidation current in the DPV signal was observed. Recently, Mohammed et al.¹⁵⁰ also used MB as a redox indicator radiator in which the fabricated biosensor comprised gold nanoparticles (AuNPs) and decorated ZnO/Aptes/SiO₂.

The hybridisation of AuNPs with 3-D ZnO has opened up a new avenue for DNA biosensors. Recently, Fang et al.¹⁵¹ used AuNPs to enhance the electron transfer inside the sensor structure layer by coating it homogeneously onto 3-D ZnO-Chitosan/GCE. The chitosan layer possessed a good adhesion characteristic due to its rich amino groups, which can provide many active sites for AuNPs immobilisation. Furthermore, hydrothermal 3-D ZnO possesses a large surface area and a pore volume of 117.36 $\text{m}^2 \text{g}^{-1}$ and 0.50 $\text{cm}^3 \text{g}^{-1}$, respectively. These topographical features associated with chitosan provided a better matrix assay for AuNPs immobilisation; thus enhancing the immobilisation process of the ssDNA probe. The as-described electrochemical biosensor exhibited good sensitivity and selectivity towards the ssDNA targets over a concentration ranging from 0.00001 to 0.1 nM, with a low detection limit of up to 0.002 pM being obtained. Another recent work was reported by Perumal et al. who detected the *Leptospira* pathogen.⁴¹ As shown in Fig. 9a, 3-D ZnO nanostructures were prepared on an interdigitated electrode (IDE) and were then hybridised with AuNPs using sputtering. After that, a thiolated probe ssDNA was immobilised on the nanocomposite before being functionalised with the target DNA. The study expected the cooperation of AuNPs with the 3-D ZnO to reduce the surface defect, as the surface area increased. As a result, high binding strength and good stability of the immobilised DNA probe with 3-D ZnO were achieved. Instead of enhancing the

surface chemical functionalisation, the AuNPs possess an anti-oxidative characteristic that maintains the ZnO performance, as it easily reacts with O_2 from ambient surroundings. According to Fig. 9b, the as-prepared biosensor exhibited high selectivity towards the target DNA. In this case (for the leptospirosis disease), the pathogen gene and non-pathogen gene, which is *L. Biflexa*, were successfully distinguished; therefore, proving the good achievement of the particular work. So far, this electrochemical biosensor only lost less than 10% of its original R_{ct} value for 10 generations and hybridisations (inset: Fig. 9c).

Next, Perumal et al.⁴¹ proposed a sensing mechanism consisting of AuNPs coated with a 3-D ZnO hybrid for DNA detection supported by information from Wang et al.,¹⁵² Shan et al.,¹⁵³ Gogurla et al.,¹⁵⁴ Kashif et al.,¹⁵⁵ and Hakkinen.¹⁵⁶ This review provides a schematic image in Fig. 10 to help readers better understand this principle. Firstly, the large surface area of pure 3-D ZnO nanostructures is susceptible to ambient condition, as it can readily absorb oxygen molecules from the outside environment; thus, creating a depletion region inside the 3-D ZnO surface due to the movement of electrons from the conduction band of the nanostructures to the oxygen molecules. As a result, the nanostructure conductivity is reduced. After that, the AuNPs (gold has a higher Fermi level (5.1 eV) than ZnO) is coated onto the 3-D ZnO nanostructures, inducing the migration of electrons from AuNPs to ZnO until there is no net change in both systems. This condition leads to a reduction in the depletion region in the 3-D ZnO nanostructures system; thus, enhancing their conductivity and subsequently forming an ohmic junction at the Au/ZnO contact

point. The sulphur molecules of the complementary target and the immobilised thiolated probe DNA had covalently bonded with the AuNPs after their incubation on the device sensing area under a few hours. This negative charge of the nucleic acid tends to amend the dynamic equilibrium of the AuNPs/3-D ZnO system due to an increase in the electron-hole current density on the semiconductor surface. This condition resulted in the reduction of electron carrier concentration and led to a wide broadening of the system's depletion region again.

The functionalisation of 3-D ZnO is not limited to AuNPs. Zhang et al.¹⁵⁷ polymerised poly(indole-5-carboxylic acid) (PICA) with the 3-D ZnO nanocomposite using a potentiostat method. The biosensor has proven useful for determining the breakpoint cluster region gene and the cellular abl (BCR/ABL) fusion gene from chronic myelogenous leukaemia. When the immobilised biosensor was analysed with impedance spectroscopy, the charge transfer resistance (R_{ct}) was observed to increase (compared to an unimmobilised biosensor) due to the electrostatic repulsion caused by the electro-negative phosphate skeleton of the DNA. Further increases in R_{ct} after the hybridisation process were caused by an increment in the negatively charged phosphate skeleton of the target ssDNA. However, when PICA was used, a different situation occurred. The conducting polymer was able to enhance the current acting on the hybridisation, as it possessed a self-redox signal, which could serve as a platform for direct DNA detection.¹⁵⁸ Another hybrid work was that of Zhang et al. which coated the graphite microfiber with 3-D ZnO using the hydrothermal method. The study proposed a cost-effective approach, which improved the sensing performance of the 3-D ZnO.¹³

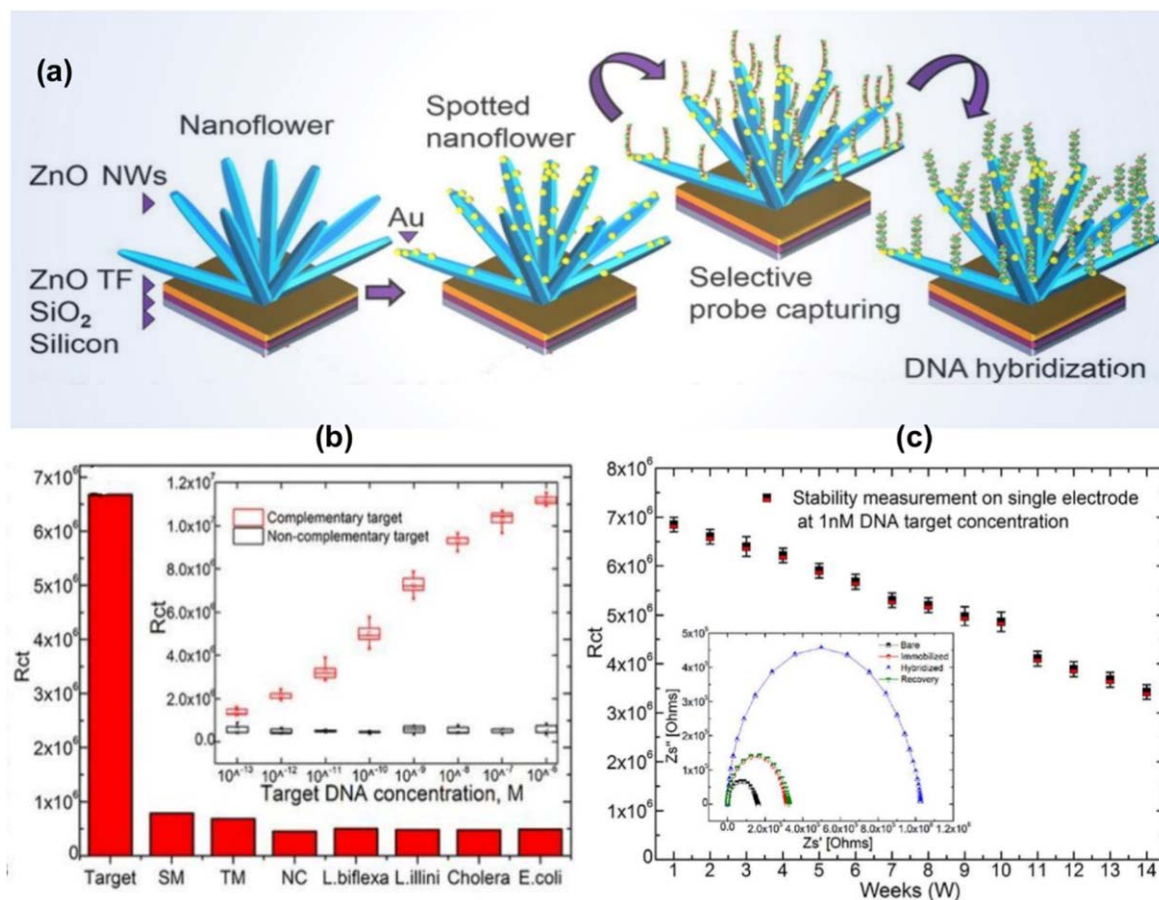


Figure 9. (a) Preparation steps of AuNPs coated on ZnO nanoflowers with the immobilisation of the ssDNA probe subsequently hybridised with the complementary target ssDNA. The ZnO nanoflowers were synthesised using a hydrothermal method while the AuNPs were deposited onto the ZnO nanoflower using sputtering; (b) the R_{ct} value of the different target analytes (inset: a graph plot of R_{ct} vs the target ssDNA concentration for complementary and non-complementary targets); (c) Long-term monitoring for the as-prepared biosensor in 14 weeks (inset: the Nyquist plot of 10 regenerations of the as-prepared biosensor device) (reprinted from, Ref. 41 © Nature Publishing Group 2015).

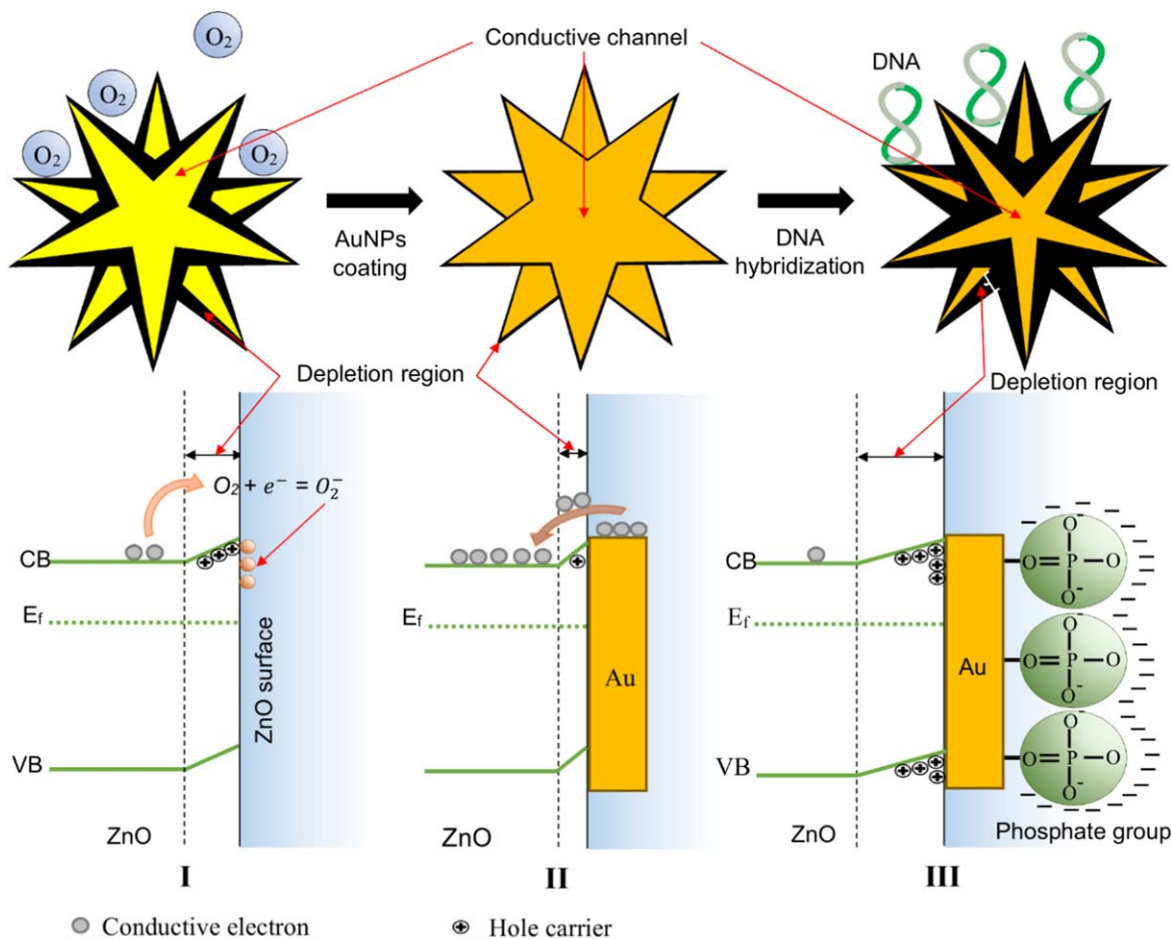


Figure 10. Schematic illustration of sensing mechanism of AuNPs coated 3-D ZnO based electrochemical sensor toward *Leptospira* DNA. (I) 3-D ZnO without coating, (II) 3-D ZnO with AuNPs coating in dynamic equilibrium and (III) Immobilized thiolated probe DNA on 3-D ZnO/AuNPs perturbs the dynamic equilibrium.

A lack of research attention on the use of silver nanoparticles (AgNPs) to incorporate in the 3-D ZnO has been observed, with only one being recorded, namely Yang et al.¹⁵⁹ The study used a bacteria protein as a target analyte, not its gene (as previously discussed in this section). Furthermore, this is the first study of its kind in which a nanostructure-based biosensor was constructed to simultaneously detect, eliminate, and deactivate the bacteria. Interestingly, the bacteria were killed by Ag^+ ions released from the AgNPs. Besides, the rapid early detection of the Zika virus using Zika nonstructural protein 1-antigen as a biomarker was also reported in Faria and Mazon.⁷ In the study, 3-D ZnO nanostructures were grown on a Printed Circuit Board using chemical bath deposition and then assembled as a portable biosensor device. The device exhibited the rapid detection of real samples without interference by the dengue virus indicated the high specificity of the biosensor. Therefore, the 3-D ZnO nanocomposite-based electrochemical biosensor is a greatly promising device for sensitively detecting infectious bacteria, either in nucleic acid or protein form. In the case of sensing bacteria in protein form, expensive cost is incurred due to the bacteria preparation. Hence, only a few works were able to use this method compared to the ssDNA. However, it should be noted that the electrochemical biosensor has some limitations in practical analyses. For example, its extremely low detection levels such as in Femto molarity concentration have forced researchers to construct nanostructure-based biosensors that exhibit a stable current in nanoscale. The nanostructure must have high resistance so it can perform sensing measurements in nano current value. This issue leads to other parameters that need to be considered, as the nanostructure can

easily be hindered by oxygen molecules from the ambient environment and the photons from a light source.

Future Prospects

Following the above discussion, it is clear that the synthesis approach, mainly the solution approach for 3-D ZnO was reviewed. Various strategies have been proposed to produce the optimum performance of nanostructures in biological sensing applications. However, with the advancements in nanotechnology and nanomaterials, some critical issues have been identified that can further improve the biosensing device. The current challenge is to produce a well-controlled dimension for 3-D subunits and morphologies. In this way, repetitive sensing measurements can be approximately 100% accurate. So far, the top-down approach using lithography can control a positioning of 3-D structure, but it still cannot control the subunit structure morphology very well. Another promising aspect is the use of a green synthesis approach. The use of plants, microorganisms, and organic material has become a vital issue for minimising hazardous chemical usage in the biosensor fabrication process. Also, more works have reported the synthesis of 3-D ZnO formation but for different applications than healthcare diagnosis, as discussed above.

Various works on biological analyte detection have been demonstrated in this review. However, many more works are expected to appear in the future. Moreover, the interaction between 3-D ZnO with different subunit nanostructures and various biological analytes still requires extensive studies. The combination of

Table II. Summary of different biomolecules detection using electrochemical biosensor based on 3-D ZnO nanostructures since 2014.

3-D Morphology	Sub-unit morphology	Hybrid/doping	Analyte	Sensing performance: Sensitivity (S), limit of detection (LOD), linear range (LR) and time response (t)
Spherical lamellar D: 2–3 μm ¹¹⁶	Nanosheet	Gold nanoparticle	Glucose	S: 1.409 $\mu\text{A mM}^{-1}$ LOD: 20 μM LR: 1–20 mM
Plant-like ¹¹⁵	Nanorod	Au and Chitosan	Glucose	S: 3.12 $\mu\text{A mM}^{-1}$ LR: 50–400 mg dl ⁻¹
Core-shell ¹⁶⁰	Nanoparticle D: 30 nm	Copper oxide	Glucose	S: 1217.4 $\mu\text{A cm}^{-2} \text{mM}^{-1}$ LOD: 1.677 μM LR: 0.02–4.86 mM
Microspheres D: 0.8–1.2 μm ¹¹⁰	Nanosheet	N/A	Glucose	S: 210.8 $\mu\text{A mM}^{-1} \text{cm}^{-2}$ LOD: 50 μM LR: 0.05–23 mM t: 3 s
Micro-pompon D: ~200 μm ¹¹²	Nanowire D: 500 nm L: 100–200 μm	Chitosan	Hydrogen peroxide	S: 1395.64 $\mu\text{A mM}^{-1} \text{cm}^{-2}$ LR: 0.2–3.4 mM
Flower ¹¹⁷	Nanowire D: 50–90 nm	Silver nanoparticle	Hydrogen peroxide	S: 50.8 $\mu\text{A mM}^{-1} \text{cm}^{-2}$ LOD: 2.5 μM (S/N = 3) LR: 1–20 μM t: <3 s
Spherical D: 2–3 μm ¹²⁹	Nanosheet	Gold nanoparticle	Dopamine	S: 210.8 $\mu\text{A mM}^{-1} \text{cm}^{-2}$ LOD: 0.02 μM (S/N = 3) LR: 0.1–300 μM t: 3 s
Flower D: 2 μm ¹³⁰	Nanoflake	Polyaniline & reduced graphene oxide	Dopamine	LOD: 0.8 nM (S/N = 3) LR: 0.001–1 μM and 1–1000 μM
			Uric acid	LOD: 0.042 μM (S/N = 3) LR: 0.1–100 μM and 100–1000 μM
Flower ¹³³	Nanowire D: 2.5 μm L: 50 nm	Indium doped tin oxide & nafion	Levadopa	S: 0.10 $\mu\text{A } \mu\text{M}^{-1}$ LOD: 2.5 μM LR: 2.5–4.0 μM
Spherical/ball D: 2 μm ¹³¹	Nanosheet T: 50 nm	Graphene foam	Dopamine	S: 0.99 $\mu\text{A } \mu\text{M}^{-1}$ LOD: 0.01 μM (S/N = 3) LR: 1–80 μM
Flower D: 2.5 μm ¹³⁴	Nanowire D: 2.5 μm L: 50 nm	Graphene & indium doped tin oxide	Levadopa	S: 0.32 $\mu\text{A } \mu\text{M}^{-1}$ LOD: 1 μM
Flower D: 2 μm ¹³⁵	Needle- shaped nanorod L: 150 nm	Reduced graphene oxide & indium doped tin oxide	Levadopa	S: 0.66 $\mu\text{A } \mu\text{M}^{-1}$ LOD: 1 μM LR: 1–60 μM
Spherical D: 2 μm ¹³²	Nanosheet T: 100 nm	Graphene foam	Levadopa	S: 0.66 $\mu\text{A } \mu\text{M}^{-1}$ LOD: 1 μM LR: 1–75 μM
Flower D: 2–3 μm ¹⁵¹	Nanosheet	Gold nanoparticle & chitosan	ssDNA	LOD: 0.002 pM LR: 0.00001–0.1 nM
Flower D: 6–8 μm ¹⁴⁶	Nanorod D: 100 nm L: 2.5 μm	N/A	ssDNA of bacteria Meningitis	S: 168.64 $\mu\text{A ng}^{-1}$ LOD: 5 ng μl^{-1} LR: 5–240 ng μl^{-1}
Flower ⁴¹	Nanorod L: 2–3 μm D: 100 nm	Gold nanoparticle	ssDNA of Leptospira	LOD: 100 fM
Flower ¹⁵⁷	Nanosheet	Poly (indole-5-carboxylic acid)	ssDNA of cluster region & cellular abl	LOD: $2.2 \times 10^{-16} \text{ M}$ LR: $1.0 \times 10^{-15} - 1.0 \times 10^{-9} \text{ M}$
Flower ⁷	Nanorod	N/A	Zika virus NS1 protein	LOD: 1.0 pg ml ⁻¹ LR: 0.1 ng ml ⁻¹ to 100 ng ml ⁻¹

Abbreviation: D: Diameter of nanostructure, L: Length of nanostructure, T: Thickness of nanostructure layer.

low and high dimensionalities of ZnO structures has opened up a new way of miniaturising and optimising sensing devices that could measure the current signal in nano values during sensing. This

advancement has made it possible to more accurately measure specific and sensitive electrical properties at low concentrations of biomolecules up to nano and femto molarity. Good sensitivity and

selectivity in detecting substances in very small concentrations, especially the DNA of infectious diseases without hindrance from foreign ions/molecules still require further investigation. Some other issues also need to be focused on such as the lack of attention in utilising 3-D ZnO in enzyme-free biosensors. This fourth-generation biosensor offers broad advantages such as low cost, low time-consuming preparation without enzyme immobilisation, good stability, and eco-friendly properties, indicating it could have a great demand and potential in this field. Indeed, growing research interest into 3-D ZnO-based electrochemical biosensors will continue with the increasing prevalence of health issues and advancements in the theoretical aspects of this field. The experimental expertise acquired through investigations into 3-D ZnO-based electrochemical biosensors could be extended to the overall biosensor industry.

Conclusions

This review briefly summarised the used of 3-D ZnO-based electrochemical biosensors in healthcare diagnosis. In recent years, a lot of improvements have been achieved in the construction of advance structures of composite-based electrochemical biosensors consisting of 3-D ZnO and another nanomaterials to enhance the biosensor performance. Fabricating the three dimensionalities of ZnO is advantageous for the immobilisation of bioreceptors such as enzymes, antibodies, and nucleic acid. The synergetic formation of the aggregation of various low-dimensional ZnO as subunits has made nanostructures a potential platform for facilitating biological sensing reactions. These advances starting from 2014 have led to the detection of more and more analytes in human healthcare diagnosis using 3-D ZnO-based electrochemical biosensors, the works of which are listed in Table II. It is not possible to address all of the recent works in this review. However, we have attempted to cover 3-D ZnO nanostructures based electrochemical biosensors, considering the morphological aspects, pore and defect effect along with various biomolecules detection including glucose, cholesterol, electroactive species, and DNA of infectious disease such as bacteria and virus.

Acknowledgments

The authors gratefully acknowledge the financial support from Research University grant of Universiti Teknologi Malaysia GUP Tier 2, vot No. 16J17. The authors would like to acknowledge the support from Micro-Nano Systems Engineering Laboratory, School of Electrical Engineering, UTM and University-Industry Research Lab of UTM.

ORCID

Suhana Mohamed Sultan  <https://orcid.org/0000-0003-1853-4476>

References

- R. Ahmad, N. Tripathy, M.-S. Ahn, and Y.-B. Hahn, *Sci. Rep.*, **7**, 46475 (2017).
- Y. Zhao et al., *Sci. Rep.*, **6**, 32327 (2016).
- X. Li, C. Zhao, and X. Liu, *Microsyst. Nanoeng.*, **1**, 15014 (2015).
- R. Ahmad, N. Tripathy, and Y.-B. Hahn, *Sensors Actuators, B: Chem.*, **169**, 382 (2012).
- N. R. Shanmugam, S. Muthukumar, and S. Prasad, *Sci. Rep.*, **6**, 33423 (2016).
- S. M. U. Ali, Z. H. Ibupoto, M. Kashif, U. Hashim, and M. Willander, *Sensors*, **12**, 2787 (2012).
- A. M. Faria and T. Mazon, *Talanta*, **203**, 153 (2019).
- G. Congur, E. S. Ates, A. Afal, H. E. Unalan, and A. Erdem, *J. Am. Ceram. Soc.*, **98**, 663 (2015).
- D. Sakai et al., *Sci. Rep.*, **9**, 14160 (2019).
- T. Tharsika, A. Haseeb, S. Akbar, and M. Thanihaichelvan, *Ceram. Int.*, **41**, 5205 (2015).
- Z. Ye, T. Wang, S. Wu, X. Ji, and Q. Zhang, *J. Alloys Compd.*, **690**, 189 (2017).
- S. B. Rana, R. Singh, and S. Arya, *J. Mater. Sci., Mater. Electron.*, **28**, 2660 (2017).
- J. Zhang, D. Han, R. Yang, Y. Ji, J. Liu, and X. Yu, *Bioelectrochem.*, **128**, 126 (2019).
- Y. Ya, C. Jiang, T. Li, J. Liao, Y. Fan, Y. Wei, F. Yan, and L. Xie, *Sensors*, **17**, 545 (2017).
- X. Wang, M. Ahmad, and H. Sun, *Materials*, **10**, 1304 (2017).
- L. Reverté, B. Prieto-Simón, and M. Campàs, *Anal. Chim. Acta*, **908**, 8 (2016).
- H. A. Abdulbari and E. A. Basheer, *ChemBioEng Rev.*, **4**, 92 (2017).
- H. Heydari, M. B. Gholivand, and A. Abdolmaleki, *Mater. Sci. Eng. C*, **66**, 16 (2016).
- Y. Li, Y. Liu, J. Liu, J. Liu, H. Tang, C. Cao, D. Zhao, and Y. Ding, *Sci. Rep.*, **5**, 7699 (2015).
- Y. Zhang, J. Xiao, Q. Lv, L. Wang, X. Dong, M. Asif, J. Ren, W. He, Y. Sun, and F. Xiao, *ACS Appl. Mater. Interfaces*, **9**, 38201 (2017).
- R. Ahmad, N. Tripathy, S. H. Kim, A. Umar, A. Al-Hajry, and Y.-B. Hahn, *Electrochem. Commun.*, **38**, 4 (2014).
- R. Ahmad, N. Tripathy, and Y.-B. Hahn, *Biosens. Bioelectron.*, **45**, 281 (2013).
- N. P. Shetti, S. D. Bukkitgar, R. R. Kakarla, C. Reddy, and T. M. Aminabhavi, *Biosens. Bioelectron.*, **141**, 111417 (2019).
- T. Kavitha, A. I. Gopalan, K.-P. Lee, and S.-Y. Park, *Carbon*, **50**, 2994 (2012).
- M. L. M. Napi, S. M. Sultan, R. Ismail, K. W. How, and M. K. Ahmad, *Materials*, **12**, 2985 (2019).
- S. M. Sultan, M. R. R. de Planque, P. Ashburn, and H. M. H. Chong, *J. Nanomater.*, **2017**, 7 (2017).
- M. W. Shinwari, D. Zhitomirsky, I. A. Deen, P. R. Selvaganapathy, M. J. Deen, and D. Landheer, *Sensors*, **10**, 1679 (2010).
- B. R. Eggins, *Chemical Sensors and Biosensors* (John Wiley & Sons Ltd, West Sussex) (2008).
- A. Tarasov, D. W. Gray, M.-Y. Tsai, N. Shields, A. Montrose, N. Creedon, P. Lovera, A. O'Riordan, M. H. Mooney, and E. M. Vogel, *Biosens. Bioelectron.*, **79**, 669 (2016).
- L. Cui, J. Wu, and H. Ju, *Biosens. Bioelectron.*, **63**, 276 (2015).
- Y.-W. Hsu, T.-K. Hsu, C.-L. Sun, Y.-T. Nien, N.-W. Pu, and M.-D. Ger, *Electrochim. Acta*, **82**, 152 (2012).
- M. Shukla, T. Dixit, R. Prakash, I. Palani, and V. Singh, *Appl. Surf. Sci.*, **422**, 798 (2017).
- D. Grieshaber, R. MacKenzie, J. Vörös, and E. Reimhult, *Sensors*, **8**, 1400 (2008).
- S. A. Prerna, A. Sharma, B. Singh, A. Tomar, S. Singh, and R. Sharma, *Integr. Ferroelectr.*, **205**, 1 (2020).
- D. Solís, F. D. P. M. Jiménez, R. S. Schreblor, E. N. Astorga, M. C. L. Escalante, J. J. P. Pérez, J. R. R. Barrado, and E. A. Dalchiale, *J. Electrochem. Soc.*, **167**, 112504 (2020).
- C.-L. Hsu, Y.-J. Fang, T.-J. Hsueh, S.-H. Wang, and S.-J. Chang, *J. Phys. Chem. B*, **121**, 2931 (2017).
- M. Kumar, B. E. K. Swamy, S. Reddy, J. K. S. Kumara, and W. Zhao, *J. Electrochem. Soc.*, **167**, 087511 (2020).
- J. N. Tiwari, R. N. Tiwari, and K. S. Kim, *Prog. Mater. Sci.*, **57**, 724 (2012).
- C. Lei, M. Pi, C. Jiang, B. Cheng, and J. Yu, *J. Colloid Interface Sci.*, **490**, 242 (2017).
- A. Mohammadzadeh, M. Azadbeh, B. Shokriyan, and S. N. K. Abad, *Ceram. Int.*, **46**, 2552 (2020).
- V. Perumal, U. Hashim, S. C. Gopinath, R. Haarindraprasad, K. Foo, S. Balakrishnan, and P. Poopalan, *Sci. Rep.*, **5**, 12231 (2015).
- J. Zhao et al., *J. Electrochem. Soc.*, **166**, H3074 (2019).
- L. Wang, Q. Xiong, F. Xiao, and H. Duan, *Biosens. Bioelectron.*, **89**, 136 (2017).
- R. Ahmad, T. Mahmoudi, M.-S. Ahn, and Y.-B. Hahn, *Biosens. Bioelectron.*, **100**, 312 (2018).
- R. Batool, A. Rhouti, M. H. Nawaz, A. Hayat, and J. L. Marty, *Biosensors*, **9**, 46 (2019).
- C. Zhu, G. Yang, H. Li, D. Du, and Y. Lin, *Anal. Chem.*, **87**, 230 (2014).
- A. M. Faria, E. B. M. I. Peixoto, C. B. Adamo, A. Flacker, E. Longo, and T. Mazon, *Sci. Rep.*, **9**, 7411 (2019).
- S. Chawla, R. Rawal, D. Kumar, and C. S. Pundir, *Anal. Biochem.*, **430**, 16 (2012).
- B. Fang, C. Zhang, W. Zhang, and G. Wang, *Electrochim. Acta*, **55**, 178 (2009).
- J. Li, W. Zhang, and J. Sun, *Ceram. Int.*, **42**, 9851 (2016).
- R. Wu, X. Chen, and J. Hu, *J. Solid State Electr.*, **16**, 1975 (2012).
- J. Zhao, F. Mu, L. Qin, J. Jia, and C. Yang, *Mater. Chem. Phys.*, **166**, 176 (2015).
- N. Batra, M. Tomar, and V. Gupta, *Biosens. Bioelectron.*, **67**, 263 (2015).
- J. Li, Y. Zhang, S. To, L. You, and Y. Sun, *ACS Nano*, **5**, 6661 (2011).
- P. R. Nair and M. A. Alam, *IEEE Trans. Electron Devices*, **54**, 3400 (2007).
- W. Suginta, P. Khunkaewla, and A. Schulte, *Chem. Rev.*, **113**, 5458 (2013).
- S. Arya, P. K. Lehana, and S. B. Rana, *J. Electron. Mater.*, **46**, 4604 (2017).
- Y.-L. Chu, S.-J. Young, L.-W. Ji, T.-T. Chu, K.-T. Lam, Y.-J. Hsiao, I. T. Tang, and T.-H. Kuo, *J. Electrochem. Soc.*, **167**, 117503 (2020).
- B. Abdallah, M. Kakhia, W. Zetoune, and N. Alkafri, *Mater. Res. Express*, **6**, 115079 (2019).
- C.-L. Hsu, J.-H. Lin, D.-X. Hsu, S.-H. Wang, S.-Y. Lin, and T.-J. Hsueh, *Sens. Actuators B Chem.*, **238**, 150 (2017).
- S.-J. Young and Y.-H. Liu, *IEEE J. Sel. Top. Quant.*, **23**, 1 (2017).
- Q. Ren, Y.-Q. Cao, D. Arulraj, C. Liu, D. Wu, W.-M. Li, and A.-D. Li, *J. Electrochem. Soc.*, **167**, 067528 (2020).
- Z. Li, Y. Xie, Y. Xiong, and R. Zhang, *New J. Chem.*, **27**, 1518 (2003).
- M. L. M. Napi, S. Sultan, R. Ismail, M. K. Ahmad, and G. Chai, *J. Nanomater.*, **2019**, 10 (2019).
- N. A. Nia, M. M. Foroughi, S. Jahani, M. S. Zandi, and N. Rastakhiz, *J. Electrochem. Soc.*, **166**, B489 (2019).
- M. Kang and H.-S. Kim, *Sci. Rep.*, **6**, 24870 (2016).
- Y. Wang, J. Yang, Y. Li, T. Jiang, J. Chen, and J. Wang, *Mater. Chem. Phys.*, **153**, 266 (2015).
- R. Krishnapriya, S. Praneetha, and A. V. Murugan, *New J. Chem.*, **40**, 5080 (2016).
- L. Zhu, W. Zeng, J. Yang, and Y. Li, *Ceram. Int.*, **44**, 19825 (2018).

70. Y. Sun, L. Wang, X. Yu, and K. Chen, *Cryst. Eng. Comm.*, **14**, 3199 (2012).
71. K. A. Eswar, J. Rouhi, F. S. Husairi, R. Dalvand, S. A. H. Alrokayan, H. A. Khan, M. R. Mahmood, and S. Abdullah, *J. Mol. Struct.*, **1074**, 140 (2014).
72. M. Navaneethan, V. Patil, S. P. Onnusamy, C. Muthamizhchelvan, S. Kawasaki, P. Patil, and Y. Hayakawa, *Sens. Actuators B Chem.*, **255**, 672 (2018).
73. B. Zhang, L. Lu, Q. Hu, F. Huang, and Z. Lin, *Biosens. Bioelectron.*, **56**, 243 (2014).
74. A. A. Ibrahim, G. Dar, S. A. Zaidi, A. Umar, M. Abaker, H. Bouzid, and S. Baskoutas, *Talanta*, **93**, 257 (2012).
75. M. R. Alenezi, S. J. Henley, N. G. Emerson, and S. R. P. Silva, *Nanoscale*, **6**, 235 (2014).
76. G. Wu, Y. Cheng, Q. Xie, Z. Jia, F. Xiang, and H. Wu, *Mater. Lett.*, **144**, 157 (2015).
77. G. Wu, Z. Jia, Y. Cheng, H. Zhang, X. Zhou, and H. Wu, *Appl. Surf. Sci.*, **464**, 472 (2019).
78. S.-J. Kim, C. W. Na, I.-S. Hwang, and J.-H. Lee, *Sens. Actuators B Chem.*, **168**, 83 (2012).
79. N. Tripathy, R. Ahmad, H.-S. Jeong, and Y.-B. Hahn, *Inorg. Chem.*, **51**, 1104 (2011).
80. A. K. Zak, W. H. A. Majid, H. Z. Wang, R. Yousefi, A. M. Golsheikh, and Z. F. Ren, *Ultrason. Sonochem.*, **20**, 395 (2013).
81. J.-F. Tang, H.-H. Su, Y.-M. Lu, and S.-Y. Chu, *CrystEngComm*, **17**, 592 (2015).
82. X. L. Li, C. X. Wang, and G. W. Yang, *Prog. Mater. Sci.*, **64**, 121 (2014).
83. M. S. Saneei Mousavi, F. Manteghi, M. Kolahdouz, R. Soleimanzadeh, M. Norouzi, and Z. Kolahdouz Esfahani, *J. Alloys Compd.*, **650**, 936 (2015).
84. H. Agarwal, S. V. Kumar, and S. Rajeshkumar, *Resour. Eff. Technol.*, **3**, 406 (2017).
85. G. Oboh, V. O. Odubanjo, F. Bello, A. O. Ademolun, S. I. Oyeleye, E. E. Nwanna, and A. O. Ademiluyi, *J. Basic Clin. Physiol. Pharmacol.*, **27**, 131 (2016).
86. P. Sharma, A. B. Jha, R. S. Dubey, and M. Pessarakli, *J. Bot.*, **2012**, 26 (2012).
87. M. Shahid and F. Mohammad, *J. Clean. Prod.*, **57**, 2 (2013).
88. M. D. Rao and P. Gautam, *Environ. Prog. Sustain. Energy*, **35**, 1020 (2016).
89. S. Azizi, M. B. Ahmad, F. Namvar, and R. Mohamad, *Mater. Lett.*, **116**, 275 (2014).
90. S. M. Sultan, K. Sun, M. R. de Planque, P. Ashburn, and H. Chong, *Solid-State Device Research Conference (ESSDERC), 2012 Proceedings of the European, Piscataway, NJ(IEEE)* p. 137 (2012).
91. Y.-J. Kim, J. Yoo, B.-H. Kwon, Y. J. Hong, C.-H. Lee, and G.-C. Yi, *Nanotechnol.*, **19**, 315202 (2008).
92. A. B. Djuricic, X. Y. Chen, and Y. H. Leung, *Recent Pat. Nanotech.*, **6**, 124 (2012).
93. W. Shi, S. Song, and H. Zhang, *Chem. Soc. Rev.*, **42**, 5714 (2013).
94. D. M. Cunha and F. L. Souza, *J. Alloys Compd.*, **577**, 158 (2013).
95. R. Idiatwiti et al., *IOP Conference Series: Materials Science and Engineering* **202** (2017) 012050.
96. S. Agarwal, P. Rai, E. N. Gatell, E. Llobet, F. Güell, M. Kumar, and K. Awasthi, *Sens. Actuators B Chem.*, **292**, 24 (2019).
97. F. V. Molefe, L. F. Koao, J. J. Dolo, and B. F. Dejene, *Physica B: Condens. Matt.*, **439**, 185 (2014).
98. J.-J. Feng, Q.-C. Liao, A.-J. Wang, and J.-R. Chen, *Cryst. Eng. Comm.*, **13**, 4202 (2011).
99. G. Katwal, M. Paulose, I. A. Rusakova, J. E. Martinez, and O. K. Varghese, *Nano Lett.*, **16**, 3014 (2016).
100. Z. Li, X. Huang, J. Liu, Y. Li, X. Ji, and G. Li, *Mater. Lett.*, **61**, 4362 (2007).
101. A. Hosseini, Z. Sheybanifard, and A. R. Mahjoub, *Inorg. Nano-Met. Chem.*, **47**, 302 (2017).
102. B. G. Shohany and A. K. Zak, *Ceram. Int.*, **46**, 5507 (2020).
103. W.-Y. Wu, W.-Y. Kung, and J.-M. Ting, *J. Am. Ceram. Soc.*, **94**, 699 (2011).
104. Y.-J. Kim, A. Yoon, M. Kim, G.-C. Yi, and C. Liu, *Nanotechnol.*, **22**, 245603 (2011).
105. Z. Yi, J. Luo, X. Ye, Y. Yi, J. Huang, Y. Yi, T. Duan, W. Zhang, and Y. Tang, *Superlattices Microstruct.*, **100**, 907 (2016).
106. N. Kumar, H. Mittal, L. Reddy, P. Nair, J. C. Ngila, and V. Parashar, *RSC Adv.*, **5**, 38801 (2015).
107. Y. Guo, S. Lin, X. Li, and Y. Liu, *Appl. Surf. Sci.*, **384**, 83 (2016).
108. S. Fan, M. Zhao, L. Ding, Y. Ma, J. Liang, X. Wang, Y. Song, and S. Chen, *Sens. Actuators B Chem.*, **237**, 373 (2016).
109. B. Fang, C. Zhang, G. Wang, M. Wang, and Y. Ji, *Sens. Actuators B Chem.*, **155**, 304 (2011).
110. R. Ahmad, N. Tripathy, M. Y. Khan, K. S. Bhat, M.-S. Ahn, G. Khang, and Y.-B. Hahn, *Ceram. International*, **42**, 13464 (2016).
111. N. Tripathy, R. Ahmad, E. Y. Kim, G. Khang, and Y.-B. Hahn, *RSC Adv.*, **4**, 46049 (2014).
112. Y. Zhou, L. Wang, Z. Ye, M. Zhao, and J. Huang, *Electrochim. Acta*, **115**, 277 (2014).
113. X. Ren, D. Chen, X. Meng, F. Tang, X. Hou, D. Han, and L. Zhang, *J. Colloid Interface Sci.*, **334**, 183 (2009).
114. C. Chen, Q. Xie, D. Yang, H. Xiao, Y. Fu, Y. Tan, and S. Yao, *RSC Adv.*, **3**, 4473 (2013).
115. K. Tian, S. Alex, G. Siegel, and A. Tiwari, *Mater. Sci. Engin. C*, **46**, 548 (2015).
116. L. Fang, B. Liu, L. Liu, Y. Li, K. Huang, and Q. Zhang, *Sens. Actuators B Chem.*, **222**, 1096 (2016).
117. M. Hussain, H. Sun, S. Karim, A. Nisar, M. Khan, A. ul Haq, M. Iqbal, and M. Ahmad, *J. Nanoparticle Res.*, **18**, 95 (2016).
118. W. Liu, W. Zhan, X. Jia, Q. Liu, R. Chen, D. Li, Y. Huang, G. Zhang, and H. Ni, *Appl. Surf. Sci.*, **480**, 341 (2019).
119. H. Tang, P. Lin, H. L. Chan, and F. Yan, *Biosens. Bioelectron.*, **26**, 4559 (2011).
120. S. Sandeep, A. S. Santhosh, N. K. Swamy, G. S. Suresh, J. S. Melo, and K. S. Nithin, *Mater. Sci. Engin. B*, **232-235**, 15 (2018).
121. B. Rezaei, L. Shams-Ghahfarokhi, E. Havakeshian, and A. A. Ensafi, *Talanta*, **158**, 42 (2016).
122. N. Smirnov, *Free Radic. Biol. Med.*, **122**, 116 (2018).
123. A. A. Abdelwahab and Y.-B. Shim, *Sens. Actuators B Chem.*, **221**, 659 (2015).
124. S. Qi, B. Zhao, H. Tang, and X. Jiang, *Electrochim. Acta*, **161**, 395 (2015).
125. D. Zhao, G. Yu, K. Tian, and C. Xu, *Biosens. Bioelectron.*, **82**, 119 (2016).
126. E. E. Ferapontova, *Electrochim. Acta*, **245**, 664 (2017).
127. J.-M. Zen and P.-J. Chen, *Anal. Chem.*, **69**, 5087 (1997).
128. C. Xia, N. Wang, L. Wang, and L. Guo, *Sens. Actuators B Chem.*, **147**, 629 (2010).
129. L. Fang, K. Huang, B. Zhang, B. Liu, Y. Liu, and Q. Zhang, *RSC Adv.*, **4**, 48986 (2014).
130. K. Ghanbari and M. Moloudi, *Anal. Biochem.*, **512**, 91 (2016).
131. S. Huang, S. Song, H. Yue, X. Gao, B. Wang, and E. Guo, *Sens. Actuators B Chem.*, **277**, 381 (2018).
132. H. Y. Yue, S. S. Song, X. R. Guo, S. Huang, X. Gao, Z. Wang, W. Q. Wang, H. J. Zhang, and P. F. Wu, *J. Electroanal. Chem.*, **838**, 142 (2019).
133. H. Y. Yue, B. Wang, S. Huang, X. Gao, X. Y. Lin, L. H. Yao, E. H. Guan, H. J. Zhang, and S. S. Song, *Ionics*, **23**, 3479 (2017).
134. H. Y. Yue, B. Wang, S. Huang, X. Gao, S. S. Song, E. H. Guan, H. J. Zhang, P. F. Wu, and X. R. Guo, *J. Mater. Sci., Mater. Electron.*, **29**, 14918 (2018).
135. H. Y. Yue, P. F. Wu, S. Huang, X. Gao, Z. Wang, W. Q. Wang, H. J. Zhang, S. S. Song, and X. R. Guo, *J. Mater. Sci., Mater. Electron.*, **30**, 3984 (2019).
136. K. M. Millan and S. R. Mikkelsen, *Anal. Chem.*, **65**, 2317 (1993).
137. C. Singhal, M. Khanuja, N. Chaudhary, C. Pundir, and J. Narang, *Sci. Rep.*, **8**, 7734 (2018).
138. M. M. Silva, A. C. Dias, B. V. Silva, S. L. Gomes-Filho, L. T. Kubota, M. O. Goulart, and R. F. Dutra, *J. Chem. Technol. Biotechnol.*, **90**, 194 (2015).
139. N. A. Mansor, Z. M. Zain, H. H. Hamzah, M. S. A. Noorden, S. S. Jaapar, V. Beni, and Z. H. Ibutoto, *Open J. Appl. Biosens.*, **3**, 9 (2014).
140. M. Das, G. Sumana, R. Nagarajan, and B. Malhotra, *Thin Solid Films*, **519**, 1196 (2010).
141. H. Karimi-Maleh, A. Bananezhad, M. R. Ganjali, P. Norouzi, and A. Sadri, *Appl. Surf. Sci.*, **441**, 55 (2018).
142. M. Chen, Y. Wang, H. Su, L. Mao, X. Jiang, T. Zhang, and X. Dai, *Sens. Actuators B Chem.*, **255**, 2910 (2018).
143. J. I. A. Rashid and N. A. Yusof, *Sens. Biosensing Res.*, **16**, 19 (2017).
144. M. K. Patel, P. R. Solanki, S. Seth, S. Gupta, S. Khare, A. Kumar, and B. Malhotra, *Electrochem. Commun.*, **11**, 969 (2009).
145. M. K. Patel, P. R. Solanki, A. Kumar, S. Khare, S. Gupta, and B. D. Malhotra, *Biosens. Bioelectron.*, **25**, 2586 (2010).
146. M. Tak, V. Gupta, and M. Tomar, *Biosens. Bioelectron.*, **59**, 200 (2014).
147. M. Tyagi, M. Tomar, and V. Gupta, *Biosens. Bioelectron.*, **41**, 110 (2013).
148. B. Liu, J. Hu, and J. S. Foord, *Electrochem. Commun.*, **19**, 46 (2012).
149. P. O. Vardevanyan, A. P. Antonyan, M. A. Parsadanyan, M. A. Shahinyan, and L. A. Hambardzumyan, *J. Appl. Spectrosc.*, **80**, 595 (2013).
150. A. M. Mohammed, I. J. Ibraheem, A. Obaid, and M. Bououdina, *Sens. Biosensing Res.*, **15**, 46 (2017).
151. L. Fang et al., *New. J. Chem.*, **38**, 5918 (2014).
152. X. Wang, X. Kong, Y. Yu, and H. Zhang, *J. Phys. Chem. C*, **111**, 3836 (2007).
153. G. Shan, M. Zhong, S. Wang, Y. Li, and Y. Liu, *J. Colloid Interf. Sci.*, **326**, 392 (2008).
154. N. Gogurla, A. K. Sinha, S. Santra, S. Manna, and S. K. Ray, *Sci. Rep.*, **4**, 6483 (2014).
155. M. Kashif, M. E. Ali, S. M. U. Ali, U. Hashim, and S. B. A. Hamid, *Nanoscale Res. Lett.*, **8**, 68 (2013).
156. H. Häkkinen, *Nat. Chem.*, **4**, 443 (2012).
157. W. Zhang, *J. Solid State Electrochem.*, **20**, 499 (2016).
158. X. Li, J. Xia, and S. Zhang, *Anal. Chim. Acta*, **622**, 104 (2008).
159. Z. Yang, Y. Wang, and D. Zhang, *Biosens. Bioelectron.*, **98**, 248 (2017).
160. B. Cai, Y. Zhou, M. Zhao, H. Cai, Z. Ye, L. Wang, and J. Huang, *Appl. Phys. A*, **118**, 989 (2015).